國 立 交 通 大 學

物理研究所

碩士論文

使用大亞灣微中子實驗探測器測量緲子散裂作用產生的中子被氫原子與釓原子俘獲之比例研究

Measurements of the Spallation Neutron Capture Rates by Hydrogen and Gadolinium Using the Daya Bay Detector

研究生：林秉言

指導教授：林貴林 教授

中 華 民 國 一 〇 三 年 七 月

國 立 交 通 大 學

物理研究所

碩士論文

使用大亞灣微中子實驗探測器測量緲子散裂作用產生的中子被氫原子與釓原子俘獲之比例研究

Measurements of the Spallation Neutron Capture Rates by Hydrogen and Gadolinium Using the Daya Bay Detector

研究生：林秉言

指導教授：林貴林 教授

中 華 民 國 一 〇 三 年 七 月

使用大亞灣微中子實驗探測器測量緲子散裂作用產生的中子被氫原子與釓原子俘獲之比例研究

Measurements of the Spallation Neutron Capture Rates by Hydrogen and Gadolinium Using the Daya Bay Detector

研 究 生：林秉言　　Student：Ping-Yen Lin

指導教授：林貴林　　Advisor：Guey-Lin Lin

國 立 交 通 大 學

物 理 研 究 所

碩 士 論 文

A Thesis
Submitted to Institute of Physics
National Chiao Tung University
in Partial Fulfillment of the Requirements
for the Degree of
Master
in
Physics

July 2014

Hsinchu, Taiwan, Republic of China

中華民國一〇三年七月

使用大亞灣微中子實驗探測器測量緲子散裂作用產生的中子被氫原子與釓原子俘獲之比例研究

學生：林秉言　　指導教授：林貴林

國立交通大學物理研究所

摘要

大亞灣反應堆微中子實驗是利用反 β 衰變測量反應堆微中子的振盪，實驗以釓原子來捕捉反 β 衰變中產生的中子，而宇宙射線緲子通過介質時所反應產生的中子被釓原子捕捉後產生的訊號是大亞灣實驗一個重要的背景。為了了解宇宙射線緲子導致的中子產量，必須分析與計算中子被釓原子捕捉的數量在中子被氫原子或釓原子捕捉的總數量中所佔之比例。我們分析了 2011 年 12 月 24 日到 2012 年 7 月 28 日的數據，得出了這個比例在六個探測器分別為：84.75%±0.3%(AD1)、84.6%±0.26%(AD2)、84.67%±0.39%(AD3)、85.11%±0.6%(AD4)、85.11%±0.56%(AD5)和 85.13%±0.59%(AD6)。

Measurements of the Spallation Neutron Capture Rates by Hydrogen and Gadolinium Using the Daya Bay Detector

Student：Ping-Yen Lin Advisor：Guey-Lin Lin

Institute of Physics
National Chiao Tung University

ABSTRACT

The Daya Bay reactor neutrino experiment measures the reactor neutrino oscillation with the inverse beta decay, where the neutron produced is captured by Gadolinium. The cosmic muon-induced neutron cause the important background for the Daya Bay experiment. To analyze the muon-induced neutron yield, calculating the neutron capture rates by Hydrogen and Gadolinium is essential. We analyze the data of 6 ADs in a period of time from December 24, 2011 to July 28, 2012. We find the rates for each AD: 84.75％±0.3％(AD1), 84.6％±0.26％(AD2), 84.67％±0.39％(AD3), 85.11％±0.6％(AD4), 85.11％±0.56％(AD5), and 85.13％±0.59％(AD6).

誌謝

謝謝指導教授林貴林老師在我就讀碩士班期間各方面的照顧與指導。

謝謝口試委員高文芳老師與王正祥老師寶貴的建議。

謝謝大亞灣合作組在技術和資源上的支援。

謝謝葉永順與胡貝禎在研究過程中，提供我技術上的引導及各方面的討論與協助。

謝謝交大物理所所有人的陪伴。

謝謝張光春、陳囿任、黃清銓、梁璐、林天宇、馬守正、姚懿恆陪我遠航。

謝謝黃昱翔與羅令崴陪伴我，鼓勵我，照顧我。

最後，謝謝我最摯愛的家人給我無條件的支持與愛護，並且信任我，讓我可以任性的做我想做的事。

林秉言(P. Y. Lin)

2014 年夏 於國立交通大學

Contents

List of Figures

List of Tables

Chapter 1

Introduction

1.1 Neutrino Physics

In 1930, Pauli proposed a new particle in order to explain the conservation law of energy-momentum and spin angular momentum in the β-decay experiment [1]. Two-body decay model of the β-decay is that a neutron decay into a proton and an electron (β particle). The emitted electron should have a fixed energy which contradict with the continuous energy spectrum in β-decay experiment by J. Chadwick in 1914 [2]. Pauli indicated that the new particle, named neutrino, is a neutral and extremely light fermion in the final state of β-decay. The spectrum of β-decay can be calculated theoretically [3] by

$$\frac{d\Gamma}{dE} = \frac{1}{\pi^3\hbar}\left(\frac{g_w}{2M_W c^2}\right)^4 E\sqrt{E^2 - m_e^2c^4}\left[(m_n - m_p)c^2 - E\right]^2 , \tag{1.1}$$

where Γ, E, g_w, M_W, m_e, m_n and m_p are total decay rate, energy of electron, weak coupling constant, W boson mass, electron mass, neutron mass and proton mass, respectively. Figure 1.1 shows the continuous energy spectrum of β-decay.

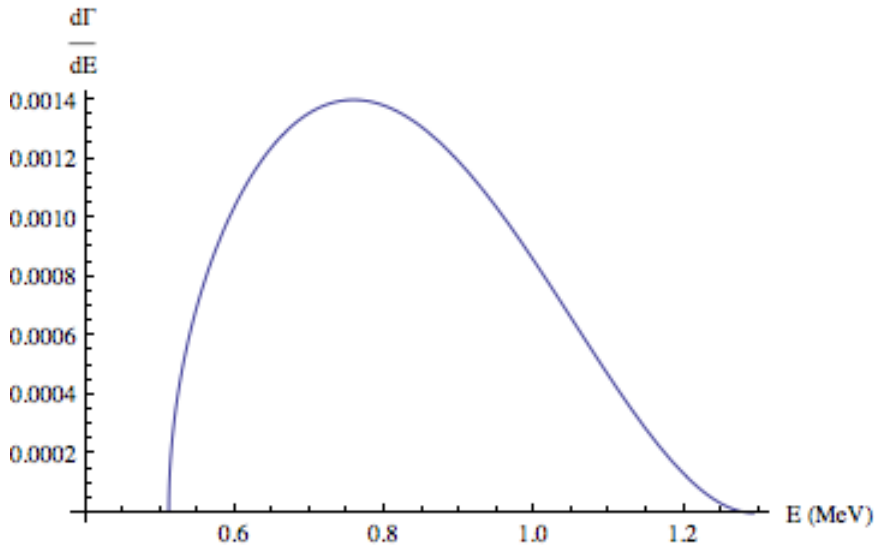

Figure 1.1: The energy spectrum of β particle in theoretical calculation.

Neutrino was first detected by Cowan and Reines in 1956 by the inverse β-decay process [4]

$$\overline{\nu}_e + p \longrightarrow e^+ + n\,, \tag{1.2}$$

where the antineutrino was produced in a reactor. In 1962, L. Lederman, M. Schwartz, and J. Steinberger discovered the muon neutrino ν_μ in Brookhaven National Laboratory [5]. The tau neutrino ν_τ was observed by Fermi National Accelerator Laboratory in 2000 [6].

In the late 1960s, it was found that the number of electron neutrino from Sun in the Homestake experiment are different from the number predicted by standard solar model [7]. The experimental number is only 1/3 of the theoretical prediction. This is so-called the solar neutrino problem. In 2001, the result of the SUDBURY Neutrino Observatory (SNO) experiment directly demonstrated the neutrino oscillation effect which implied that neutrinos are massive.

The neutrino oscillation is the quantum transition between various neutrino flavors.

The problem of neutrino oscillation is that neutrino weak eigenstates do not correspond to the neutrino mass eigenstates, but are mixture of each other. Neutrinos interact in their flavor eigenstates, but they propagate in the mass eigenstates. The transformation relating the flavor and mass eigenstates can be written as

$$|\nu_\alpha\rangle = \sum_i^\alpha U_{\alpha i}|\nu_i\rangle\,, \tag{1.3}$$

where $|\nu_\alpha\rangle$ and $|\nu_i\rangle$ represent the flavor eigenstates and the mass eigenstates of neutrino with $\alpha = e,\ \mu,\ \tau$ and $i = 1,\ 2,\ 3$, respectively. $U_{\alpha i}$ is the Pontecorvo–Maki–Nakagawa–Sakata (PMNS) mixing matrix. For three neutrino flavors, the PMNS matrix is a 3×3 unitary matrix.

$$\begin{aligned} U &= \begin{pmatrix} U_{e1} & U_{e2} & U_{e3} \\ U_{\mu1} & U_{\mu2} & U_{\mu3} \\ U_{\tau1} & U_{\tau2} & U_{\tau3} \end{pmatrix} \\ &= \begin{pmatrix} 1 & 0 & 0 \\ 0 & C_{23} & S_{23} \\ 0 & -S_{23} & C_{23} \end{pmatrix} \begin{pmatrix} C_{13} & 0 & S_{13}e^{i\delta} \\ 0 & 1 & 0 \\ -S_{13}e^{i\delta} & 0 & C_{13} \end{pmatrix} \begin{pmatrix} C_{12} & S_{12} & 0 \\ -S_{12} & C_{12} & 0 \\ 0 & 0 & 1 \end{pmatrix} \\ &\quad \times \begin{pmatrix} e^{i\alpha_1/2} & 0 & 0 \\ 0 & e^{i\alpha_2/2} & 0 \\ 0 & 0 & 1 \end{pmatrix} \end{aligned}$$

$$= \begin{pmatrix} C_{12}C_{13} & S_{12}C_{13} & S_{13}e^{-i\delta} \\ -S_{12}C_{23} - C_{12}S_{23}S_{13}e^{i\delta} & C_{12}C_{23} - S_{12}S_{23}S_{13}e^{i\delta} & S_{23}C_{13} \\ S_{12}S_{23} - C_{12}C_{23}S_{13}e^{i\delta} & -C_{12}S_{23} - S_{12}C_{23}S_{13}e^{i\delta} & C_{23}C_{13} \end{pmatrix} \times \begin{pmatrix} e^{i\alpha_1/2} & 0 & 0 \\ 0 & e^{i\alpha_2/2} & 0 \\ 0 & 0 & 1 \end{pmatrix}, \quad (1.4)$$

where $U_{\alpha i}$ is the element of transition matrix from the mass eigenstates $|\nu_i\rangle$ to the flavor eigenstates $|\nu_\alpha\rangle$, S_{ij} and C_{ij} are $\sin\theta_{ij}$ and $\cos\theta_{ij}$ with θ_{ij} the mixing angle between i and j mass eigenstate. δ, α_1 and α_2 are the CP phase and Majorana phases.

1.2 Measurement of Electron Antineutrino

The antineutrino is produced by the reactors of Daya Bay nuclear power complex. There are two near sites and one far site with eight antineutrino detectors (ADs). Two ADs are placed at each near site. Four ADs are placed at the far site for increasing the statistics. The survival probability of antineutrino was measured in order to obtain θ_{13}. The survival probability for electron antineutrino in vacuum with an energy E at a distance L is given by

$$\begin{aligned} P_{sur} &= P_{ee} = |\langle\nu_e|\nu_e(t)\rangle|^2 \\ &= 1 - \sin^2 2\theta_{13}\sin^2\frac{\Delta m^2_{31}L}{4E_\nu} - \cos^4\theta_{13}\sin^2 2\theta_{12}\sin^2\frac{\Delta m^2_{21}L}{4E_\nu} \end{aligned} \quad (1.5)$$

The ratio of the number of antineutrino events in the far site to that in the near site

is given by

$$\frac{N_f}{N_n} = \left(\frac{N_{p,f}}{N_{p,n}}\right)\left(\frac{L_n}{L_f}\right)^2\left(\frac{\epsilon_f}{\epsilon_n}\right)\left[\frac{P_{sur}(E,L_f)}{P_{sur}(E,L_n)}\right], \tag{1.6}$$

where index f and n are for far site and for near site respectively. N, N_p, L, and ϵ are measured rates, detector mass, distance to reactor, and detector efficiency, respectively. E and L_f (L_n) in P_{sur} correspond to E_ν and L in Eq. (1.5) respectively. And the value of $\sin^2 2\theta_{13}$ is approximatiely given by

$$\sin^2 2\theta_{13} \approx \frac{1}{A(E,L_f)}\left[1-\left(\frac{N_f}{N_n}\right)\left(\frac{L_f}{L_n}\right)^2\right] \tag{1.7}$$

where $A(E,L_f) = \sin^2\ \Delta_{31}$ with $\Delta_{31} \equiv 1.267\,\Delta m^2_{31}(\text{eV}^2)\times 10^3 \dfrac{L(\text{km})}{E(\text{MeV})}$ and $\Delta m^2_{31} \equiv m^2_3 - m^2_1$.

The antinutrino is detected by the inverse β-decay process in Daya Bay experiment [8]. There are two kinds of gamma ray signals for antineutrino measurement. The first signal produced by positron which is annihilated immediately, called prompt signal. A neutron is captured by proton or Gd nucleus that produced the so-call delay signal comparing to the prompt one. If the neutron is captured by a proton, a 2.2MeV gamma-ray is emitted for each event [8],i.e.

$$n + p \longrightarrow D + \gamma(2.2MeV) \tag{1.8}$$

In order to increase the neutron capture probability, a 0.1% Gd was doped in the liquid scintillator (LS) in AD. The Gd was excited by captured neutrons and returned to the

ground state by emitting 8 MeV gamma [8, 9].

$$n + Gd \longrightarrow Gd^{*} \tag{1.9}$$

$$Gd^{*} \longrightarrow Gd + \gamma(8MeV) \tag{1.10}$$

The delayed signal efficiently tags antineutrino signal. The prompt and the delayed coincidence provides a distinctive signature.

1.3 Cosmic Muon-induced Backgrounds

It is important to understanding the cosmogenic backgrounds for underground experiments. Cosmic-ray muons produce neutrons through the following mechanisms [10],

- Photo-nuclear reactions: Muons generate electromagnetic shower by Photo-nuclear reactions [11].
- Muon Spallations: Muon exchange a virtual photon with nuclei and then a neutron is produced. Figure 1.2 shows the lowest-order Feynman diagram for this interaction.

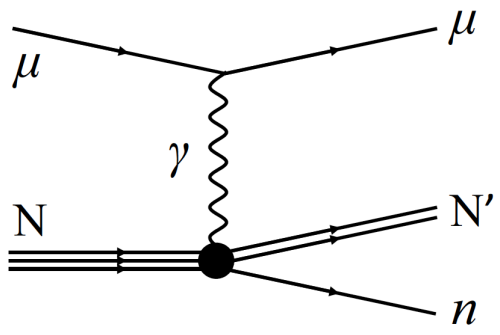

Figure 1.2: The Feynman diagram of a muon spallation process.

- Elastic scattering: Neutrons in nuclei is elastic scattered by muon.

- Secondary neutrons: The neutron production from the other neutrons produced by above processes.

- μ^- capture on nuclei: Neutrons are produced by a low energy μ^- which undergoes nuclear capture via the weak charged-current process,

$$\mu^- + A\,(Z, N) \longrightarrow \nu^{\mu} + A\,(Z-1, N+1) \tag{1.11}$$

Neutron yield is very important for neutron background estimation. The determination of the spallation neutron capture rates by Hydrogen and Gadolinium is essential for measuring the muon-induced neutron yield. The neutron yield depends on the average muon energy. We are interested in whether the H-Gd ratio also depends on the average muon energy. In previous studies by Yung-Shun Yeh, the ratio has been investigated using simulation data [10]. Table 1.1 shows his results. Here, we analyze the H-Gd capture ratio using the experimental data. The purpose of this thesis is to measure spallation neutron capture rates by Hydrogen and Gadolinium in the Daya Bay experiment.

	$\epsilon_{Gd,1}$	$\sigma_{Gd,1}$	$\epsilon_{Gd,2}$	$\sigma_{Gd,2}$
EH1	0.8552	0.0015	0.8518	0.0016
EH2	0.8526	0.0015	0.8537	0.0016
EH3	0.8548	0.0012	0.8536	0.0013

Table 1.1: The Gd-capture ratio using two different methods in Ref. [10], where ϵ_{Gd} and σ_{Gd} are Gd-capture ratio and the associated statstical uncertainty.

Chapter 2

The Daya Bay Neutrino Experiment

The Daya Bay experiment measures the rates and energy spectra of reactor electron antineutrinos at different baselines to estimate the mixing angle θ_{13} with a sensitivity of 0.01 or better in $sin^2 2\theta_{13}$ at 90% confidence level.

2.1 Experiment Layout

The Daya Bay Experiment [12] is located at the Daya Bay nuclear power complex in southern China. There are three nuclear power plants (NPPs) in the Daya Bay nuclear power complex: the Daya Bay NPP, the Ling Ao NPP and the Ling Ao II NPP. Each NPP consists of two reactor cores. The layout of the Daya Bay experiment are shown in Figure 2.1. All six cores are functionally identical reactors of 2.9 GW thermal power [12]. It gives a prolific source of reactor antineutrinos ($\sim 6 \times 10^{20} \overline{\nu}_e/s/core$).

There are three experimental halls (EHs) in the Daya Bay experiment: the Daya Bay near hall (EH1) and the Ling Ao near hall (EH2), and one far hall (EH3). All experimental halls are underground. There are mountains providing overburden to suppress cosmogenic backgrounds. Table 2.1 shows the overburden, muon rate, average muon

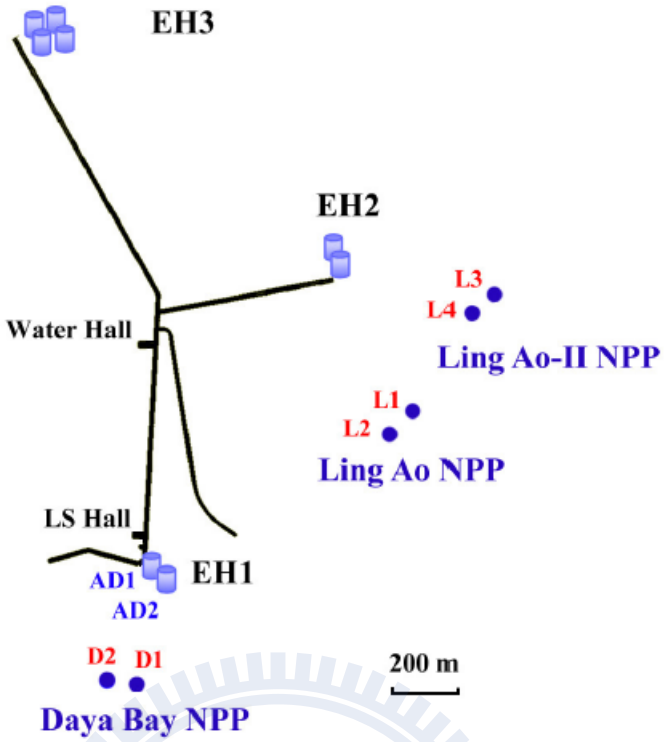

Figure 2.1: Layout of the Daya Bay experiment.

energy, and average distances to the reactor pairs for each EH, respectively. Each an-

	EH1	EH2	EH3
Overburden (m.w.e)	250	265	860
Muon rate (Hz)	1.27	0.95	0.56
Average muon energy (GeV)	57	58	137
Distance from D1/D2	364	1348	1912
Distance from L1/L2	8557	480	1540
Distance from L3/L4	1307	528	1548

Table 2.1: Site information including baselines (in meters) and overburdens. D1/D2, L1/L2, and L3/L4 stand for the reactor cores and Figure 2.1 shows the layout.

tineutrino detector (AD) is put in a water pool. The water pool shields backgrounds from the surrounding and as a detector of Cherenkov to tag cosmic-ray muons. On the top of the water pool, the resistance plate chambers (RPCs) gives an additional muon-tagging. Figure 2.2 shows the schematics of near hall. There is a similar layout with a larger water pool and RPC module array in the far hall.

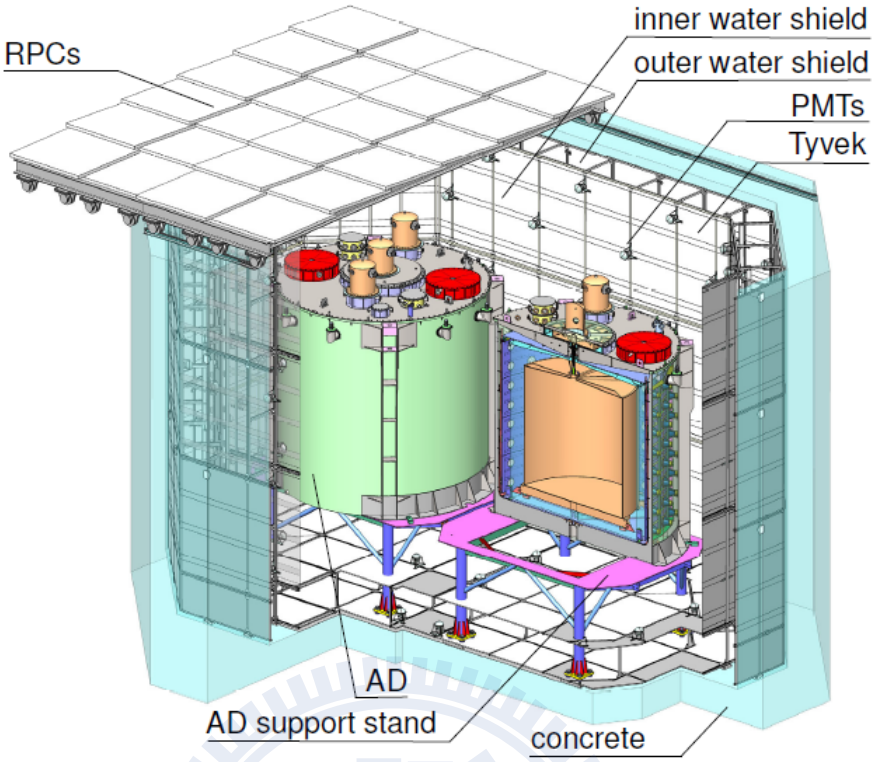

Figure 2.2: Schematic of the ADs, water shields, and RPCs in near hall.

2.2 Detectors

The structure of AD is a three-zone cylindrical vessel, which is shown in Figure 2.3. The innermost acrylic vessel (IAV) with diameters about 3 m is filled with about 20 tons of 0.1%-doped Gadolinium liquid scintillator (GdLS) as the target region. The medium zone between IAV and the outer acrylic vessel (OAV) with diameters about 4 m is filled with about 20 tons of pure liquid scintillator (LS) to capture gamma rays escaping from the target region. There are 37 tons of Mineral oil (MO) filled in the outermost zone , between the OAV and the stainless steel vessel (SSV) with diameters about 5 m, in order to avoid the entering of external radiation. All 192 8-inch photomultiplier tubes (PMTs) are installed in 8 rows (rings) and 24 columns on the inner wall of SSV with rails.

There are three Automated Calibration Units (ACUs) installed on the top of the AD as shown in Figure 2.3. The ACU-A sits on the central axis of the AD. The ACU-B

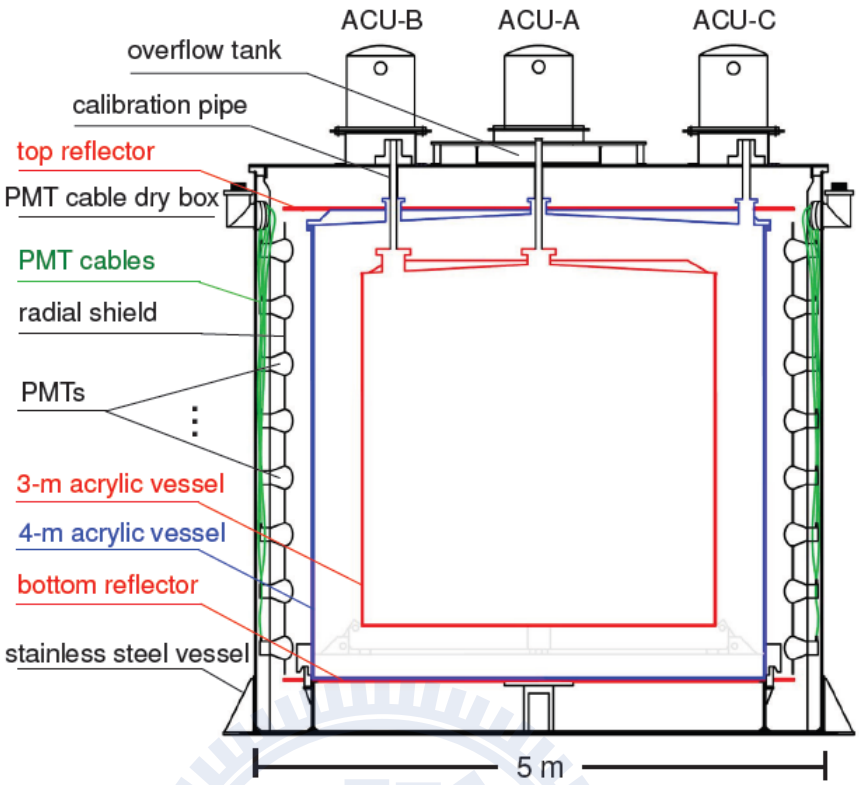

Figure 2.3: The antineutrino detector.

is designed to calibrate and study the edge effects of the IAV, and the ACU-C is used for calibrating the gamma catcher. To supplement the automated system, the manual calibration system (MCS) has been constructed. Figure 2.4 shows the MCS. The robotic arm of MCS could put the sources at any location inside the target volume through ACU-A penetration. Table 2.2 summarizes the properties of the calibration sources in ACU and MCS.

Source	Type	Energy	Half-life	Rate (Hz)	Auto/Manual System
LED	visible γ	430 nm	-	500 (adjustable)	Auto
^{68}Ge	e^+	1.022 MeV	270.95 d	10	Auto
^{60}Co	γ	2.5 MeV	1925.28 d	100	Auto and Manual
^{241}Am-^{13}C	n	$\sim$ 8 MeV*	432.6 y	$\sim$ 0.5	Auto
^{238}Pu-^{1}3C	n	$\sim$ 8 MeV*	24110 y	$\sim$ 1000	Manual

Table 2.2: Lists of calibration sources. (*) indicates the energy of capture gammas.

Most of the backgrounds come from the interactions of cosmic-ray muons with nearby materials in the Daya Bay experiment. The muon detection system include both

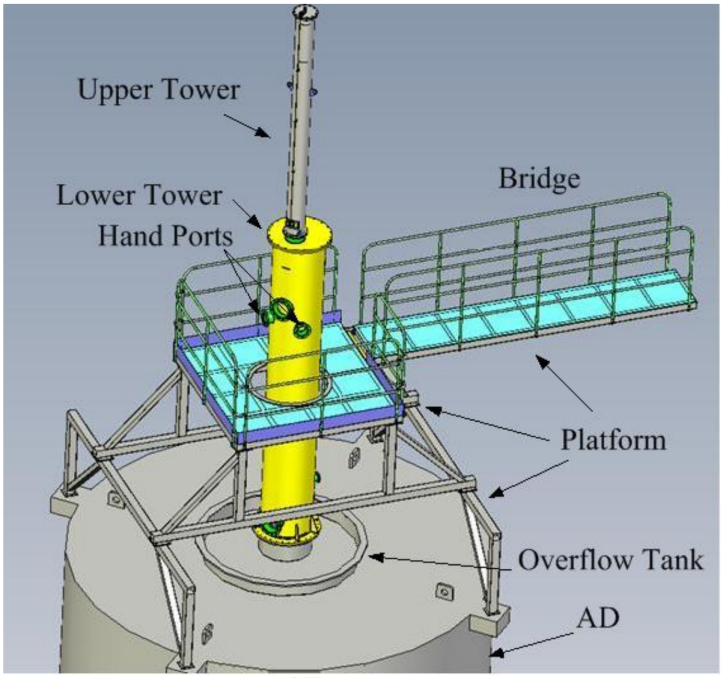

Figure 2.4: The MCS installed on the AD.

the water Cherenkov detector and the Resistive Plate Chamber detector.

To shield backgrounds from the surrounding rocks and serve as a water Cherenkov detector to tag cosmic-ray muons, the ADs is surrounded by a buffer of water with a thickness of at least 2.5 m in all directions. The water pool is divided into two parts, the inner water shield (IWS) and the outer water shield (OWS). There are 288 8-inch PMTs installed in each near hall, and 384 in the far hall.

Each water pool is covered with an array of RPC module. 54 modules are installed in both of the near halls, and 81 in the far hall. The structure of RPC is shown in Figure 2.5.

2.3 Measurement of θ_{13} and Backgrounds

The first observation of θ_{13} with a significance of 5.2 standard deviations was reported in March, 2012. The improved measurement value $\sin^2 2\theta_{13} = 0.089 \pm 0.010$ (stat.)

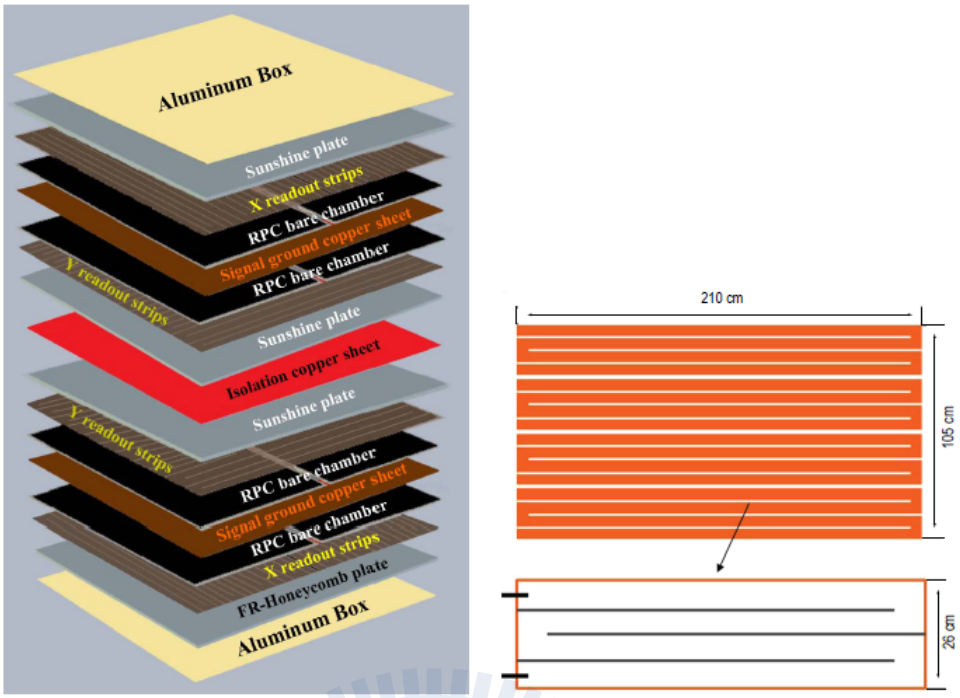

Figure 2.5: An RPC module structure.

± 0.005 (syst.) was given by Ref. [13].

2.3.1 Measurement of θ_{13}

According to the no-oscillation assumption, the $\overline{\nu}_e$ spectrum in the far hall can be predicted by a weighted combination of the two near hall measurements. The ratio R is defined as $R = M_f / \overline{N}_f$, where M_f and $\overline{N}_f$ are the measured and predicted event rates in the far hall (sum of ADs), respectively. The ratio at the far hall was [13]

$$R = 0.944 \pm 0.007 \text{ (stat.)} \pm 0.003 \text{ (syst.)}\,. \tag{2.1}$$

The energy spectra of the prompt signal and the ratio R in far hall are shown in Figure 2.6.

The best-fit value of $\sin^2 2\theta_{13}$ is determined by the χ^2 with uncorrelated systematic

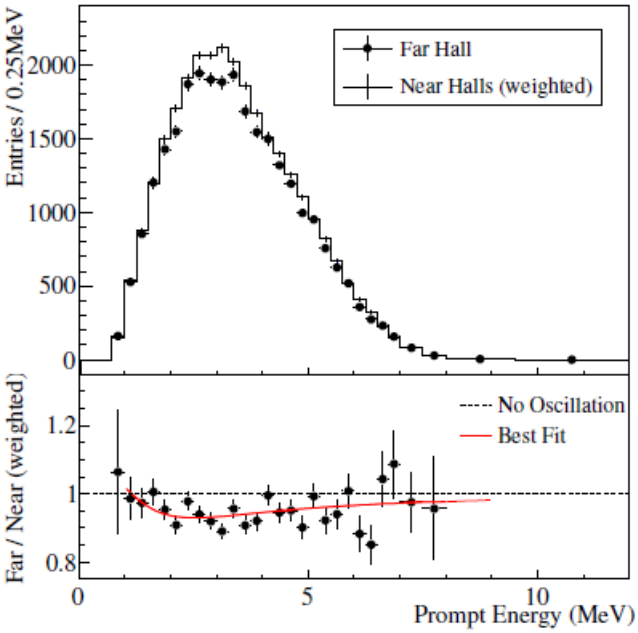

Figure 2.6: Top: measured prompt energy spectrum of the far hall (sum of ADs) compared with the no-oscillation prediction based on the measurements of the near halls. Bottom: the ratio of measured and predicted spectrum. Red solid curve is the best-fit of ratio with $\sin^2 2\theta_{13} = 0.089$, whereas the dashed curve is the non-oscillation prediction.

uncertainties defined as

$$\chi^2 = \sum_{d=1}^{6} \frac{\left[M_d - T_d\left(1+\varepsilon+\sum_r \omega_r^d \alpha_r + \varepsilon_d\right) + \eta_d\right]^2}{M_d + B_d} + \sum_r \frac{\alpha_r^2}{\sigma_r^2} + \sum_{d=1}^{6}\left(\frac{\varepsilon_d^2}{\sigma_d^2} + \frac{\eta_d^2}{\sigma_B^2}\right), \tag{2.2}$$

where M_d is the measured IBD event number of the d-th AD with its backgrounds subtracted, B_d is the corresponding background, T_d is the prediction from antineutrino flux, including MC corrections and neutrino oscillations, ω_r^d is the fraction of IBD contribution of the r-th reactor to the d-th AD determined by the baselines and antineutrino fluxes. The uncorrelated reactor uncertainty is σ_r (0.8%). The parameter σ_d (0.2%) is the uncorrelated detection uncertainty. The parameter σ_B is the quadratic sum of the background uncertainties listed in Table 2.3. The corresponding pull parameters are $(\alpha_r, \varepsilon_d, \eta_d)$. The detector- and reactor-related correlated uncertainties are not included

in the analysis. The absolute normalization ε was determined from the fitting to the data. The survival probability of $\overline{\nu}_e$ used in the χ^2 is

$$P_{\text{sur}} = 1 - \sin^2 2\theta_{13} \sin^2 \left(1.267\,\Delta m^2_{31} \frac{L}{E}\right) - \cos^4 \theta_{13} \sin^2 2\theta_{12} \sin^2 \left(1.267\,\Delta m^2_{21} \frac{L}{E}\right), \tag{2.3}$$

where $\Delta m^2_{31} = 2.32 \times 10^{-3}\,\text{eV}^2$, $\sin^2 2\theta_{12} = 0.861^{+0.026}_{-0.022}$, and $\Delta m^2_{21} = 7.59^{+0.20}_{-0.21} \times 10^{-5}\,\text{eV}^2$ [14]. The uncertainty of Δm^2_{31} [15] is not included in the fitting. The best-fit value of $\sin^2 2\theta_{13}$ with a χ^2/NDF of 3.4/4 [13] is

$$\sin^2 2\theta_{13} = 0.089 \pm 0.010(\text{stat.}) \pm 0.005(\text{syst.})\,. \tag{2.4}$$

All best estimates of pull parameters are within the one standard deviation based on the corresponding systematic uncertainties. The no-oscillation hypothesis is excluded at 7.7 standard deviations. Figure 2.7 shows the number of IBD candidates in each detector after corrections for relative efficiency and background, relative to those expected assuming no oscillation. A $\sim 1.5\%$ oscillation effect appears in the near halls, largely due to oscillation of the antineutrinos from the reactor cores in the farther cluster. The oscillation survival probability at the best-fit values is given by the smooth curve. The χ^2 value versus $\sin^2 2\theta_{13}$ is shown in the inset.

2.3.2 Backgrounds

The experiment mainly has two kinds of background, the accidental coincidence and the cosmogenic background. Below are the major backgrounds to the IBD selections:

- Accidental background: The accidental background is defined as any pair of un-

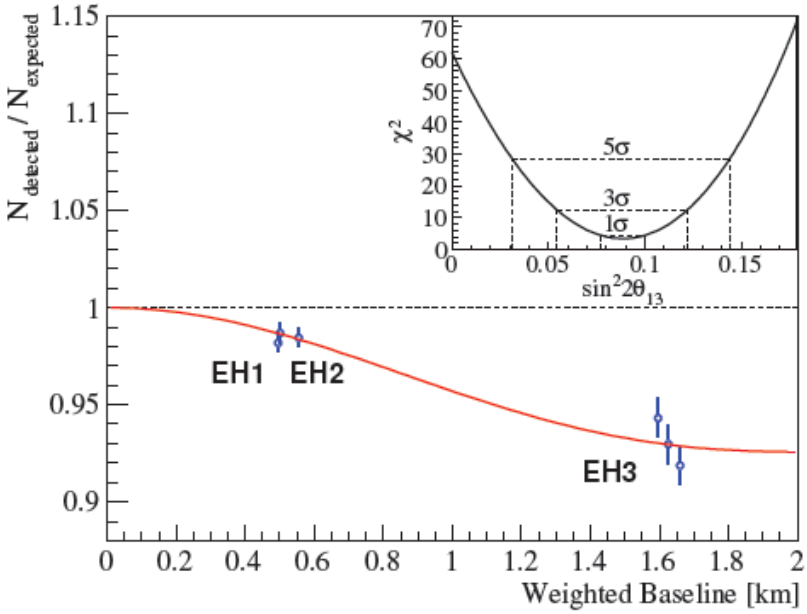

Figure 2.7: Top: Ratio of measured versus expected signals in each detector, assuming no oscillation.

correlated signals that satisfy the IBD selection criteria accidentally.

- Fast neutron background: The energetic neutrons induced by cosmic-ray muons entering the AD could mimic the prompt signal by recoiling off a proton, and give a delayed signal after being captured on Gd.

- $^{9}Li/^{8}He$ background: The rate of correlated background from the β-n cascade of the cosmogenic $^{9}Li/^{8}He$ can be estimated by evaluating the time distribution since the last muon.

- $^{1}3C(\alpha;n)^{1}6O$ background: The $^{1}3C(\alpha;n)^{1}6O$ background is determined by measuring α-decay rate in situ and then calculate the neutron yield by MC.

- Calibration source Am-C induced background: During the data taking, neutrons from the Am-C calibration source stored inside the ACU may mimic IBD events by scattering inelastically with nuclei in the shielding material, and captured on Fe, Cr, Mn or Ni in the stainless steel tank.

	AD1	AD2	AD3	AD4	AD5	AD6
IBD candidates	69121	69714	66473	9788	9669	9452
Expected IBDs	68613	69595	66402	9922.9	9940.2	9837.7
DAQ livetime (days)	127.5470		127.3763		126.2646	
ϵ_μ	0.8231	0.8198	0.8576	0.9813	0.9813	0.9810
$\overline{\epsilon}_m$	0.9738	0.9742	0.9753	0.9737	0.9734	0.9732
Accidentals (per day)	9.73±0.10	9.61±0.10	7.55±0.08	3.05 ±0.04	3.04 ± 0.04	2.93 ±0.03
Fast-neutron (per day)	0.77±0.24	0.77±0.24	0.58±0.33	0.05±0.02	0.05±0.02	0.05±0.02
^{9}Li/^{8}He (per AD per day)	2.9±1.5		2.0±1.1		0.22±0.12	
Am-C correlated (per AD per day)			0.2±0.2			
(α, n) background (per day)	0.08±0.04	0.07±0.04	0.05±0.03	0.04±0.02	0.04±0.02	0.04±0.02
IBD rate (per day)	662.47±3.00	670.87±3.01	613.53±2.69	77.57±0.85	76.62±0.85	74.97±0.84

Table 2.3: Summary of signal and background in ADs in the 3 EHs.

Chapter 3

H-Gd Ratio from Spallation Neutrons

In this Chapter, we determine the ratio of the muon-induced neutrons captured by Hydrogen and those captured by Gadolinium in the GdLS region in the 3 experimental halls of the Daya Bay experiment.

3.1 Muon-induced Neutron Production

Neutrons can be produced by the interaction between muon and the surrounding matter when a cosmic-ray muon passes through the AD. Neutrons are produced by five kinds of processes: (i) photo-nuclear interactions, (ii) muon Spallations, (iii) elastic scattering, (iv) secondary neutrons, and (v) μ^- capture on nuclei. When a neutron is captured on Gd (nGd in short), it releases gamma-rays with the total energy of about 8 MeV, whereas a neutron captured on H (nH) emits the gamma-ray with the characteristic energy about 2.2 MeV.

In order to determine the muon-induced neutron yield, it is necessary to convert the number of nGd events to the number of total neutron capture events in GdLS [10]. Hence we evaluate the ratio in this study.

3.2 Event Selection

The analysis is based on the data taken from December 24, 2011 to July 28, 2012. The data of 6 ADs deployed in 3 EHs is used. In this study, events are identified as cosmic-ray muons passing through the AD by the following selection criteria,

- AD muon (μ_{AD}): the energy deposit is greater than 20 MeV;
- WP muon (μ_{WP}): either the number of fired PMTs in IWS or OWS are greater than 12;
- μ_{AD} and μ_{WP} are within 0.3 μs.

A small number of AD PMTs spontaneously emit light due to discharge within the base. These instrumental backgrounds are referred to as flasher events.

After applying the flasher cut, events fulfilling the following criteria are selected as candidates for spallation neutrons captured on Gd,

- the time since the last muon (dT) must be located in the signal time window 20 μs $< dT <$ 300 μs, and
- the energy range is 3 sigma region around the 8 MeV peak.
- The events within $|Z| <$ 700 mm and R ($= \sqrt{X^2 + Y^2}$) $<$ 700 mm.

Any event fulfilling the following criteria is selected as the candidate for spallation neutron captured on H,

- the time since the last muon (dT) must be located in the signal time window that is defined as 20 μs $< dT <$ 300 μs, and
- the energy range is 3 sigma region around the 2.2 MeV peak.

- The events within $|Z| < 700$ mm and $R\ (= \sqrt{X^2 + Y^2}) < 700$ mm.

The lower timing cut at 20 μs is set for suppressing the effect of retrigger and ringing at the very beginning of the time period after the passing of muon[10], as depicted in Figure 3.1.

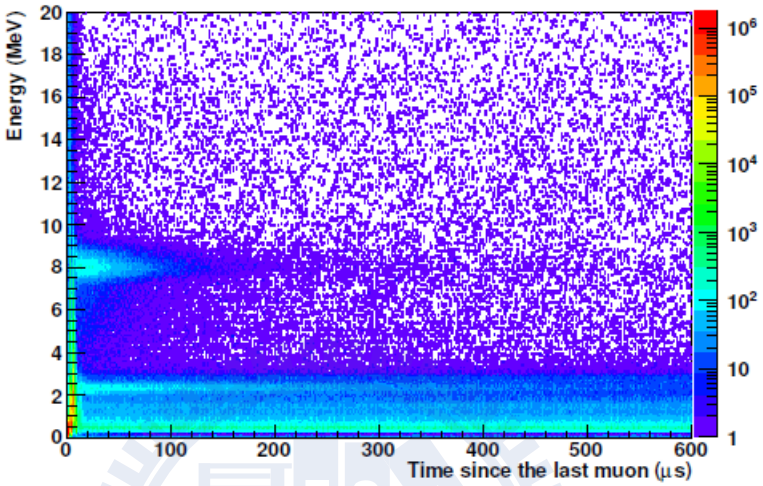

Figure 3.1: A 2D map showing the time since the last muon versus the energy of the spallation products[10].

To remove the background due to accidental coincidences, the background time window is chosen as 320 μs $< dT <$ 600 μs. Figure 3.2 shows the time since the last muon (dT), which justifies the selection of the signal time window and the background time window.

By subtracting events in the background time window from those in the signal time window (side-band subtraction in short), the accidental background can be eliminated. Figure 3.3 to Figure 3.5 show the energy spectrum in signal time window, background time window, and the energy spectrum after background subtraction, respectively.

To prevent spallation products from other muons falling on the signal time window, an isolation cut is applied such that there are no additional muon events (μ_{AD} or μ_{WP}) before 300 μs and after 610 μs of this muon event.

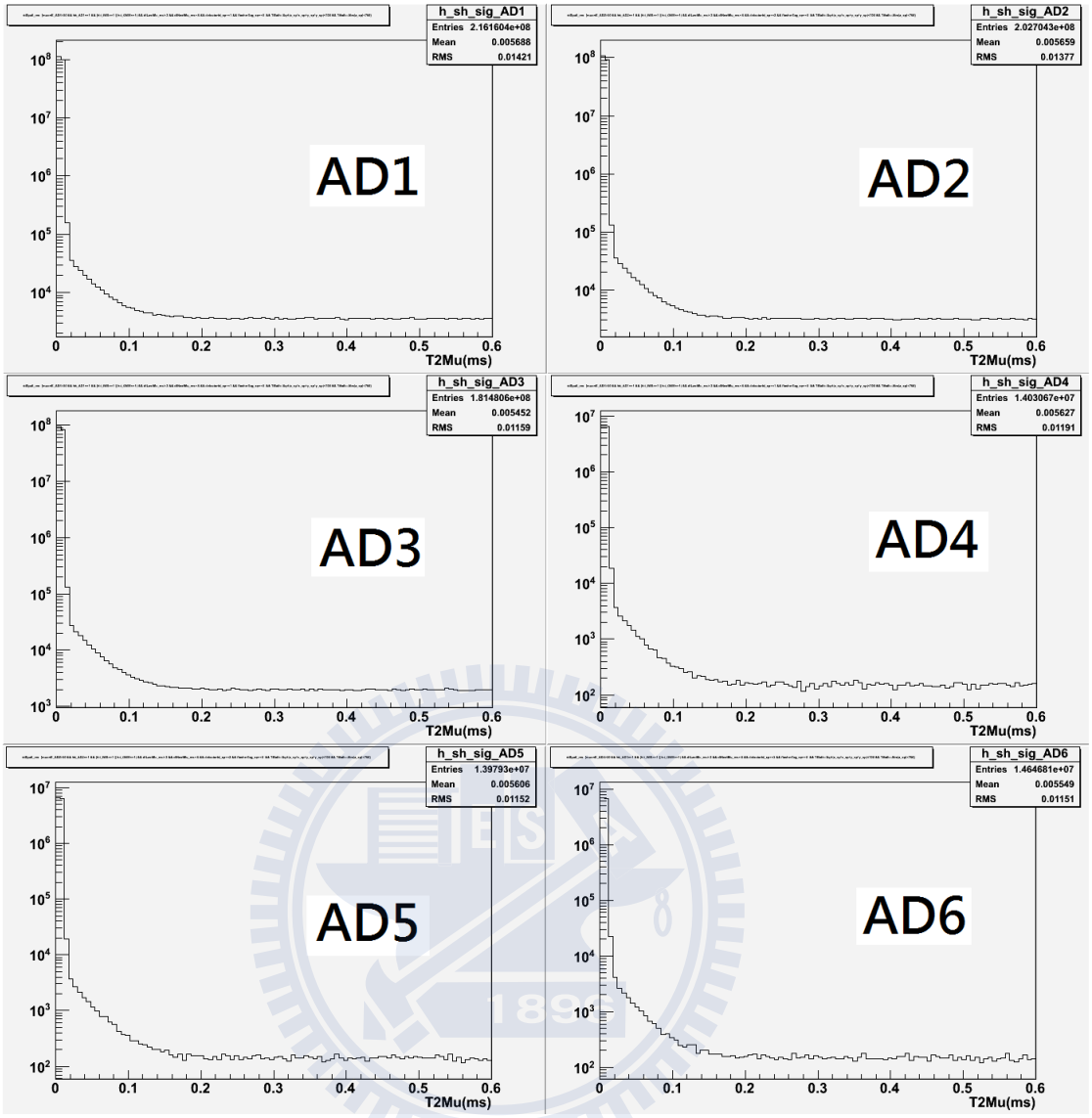

Figure 3.2: The time since the last muon (dT) for each AD. AD1 and AD2 are deployed in Daya Bay near hall, whereas AD3 is deployed in Ling Ao near hall, and the AD4 to AD6 are deployed in far hall.

3.3 H-Gd Ratio

The H-Gd ratio ($R_{\text{H-Gd}}$) is defined as

$$R_{\text{H-Gd}} = \frac{N_{\text{Gd}}}{N_{\text{total}}} = \frac{N_{\text{Gd}}}{N_{\text{H}} + N_{\text{Gd}}}, \tag{3.1}$$

where N_{Gd} is integrated around the energy at Gd-capture peak. N_{H} is integrated around H-capture peak. We determine the mean of the energy peak by fitting with Gaussian.

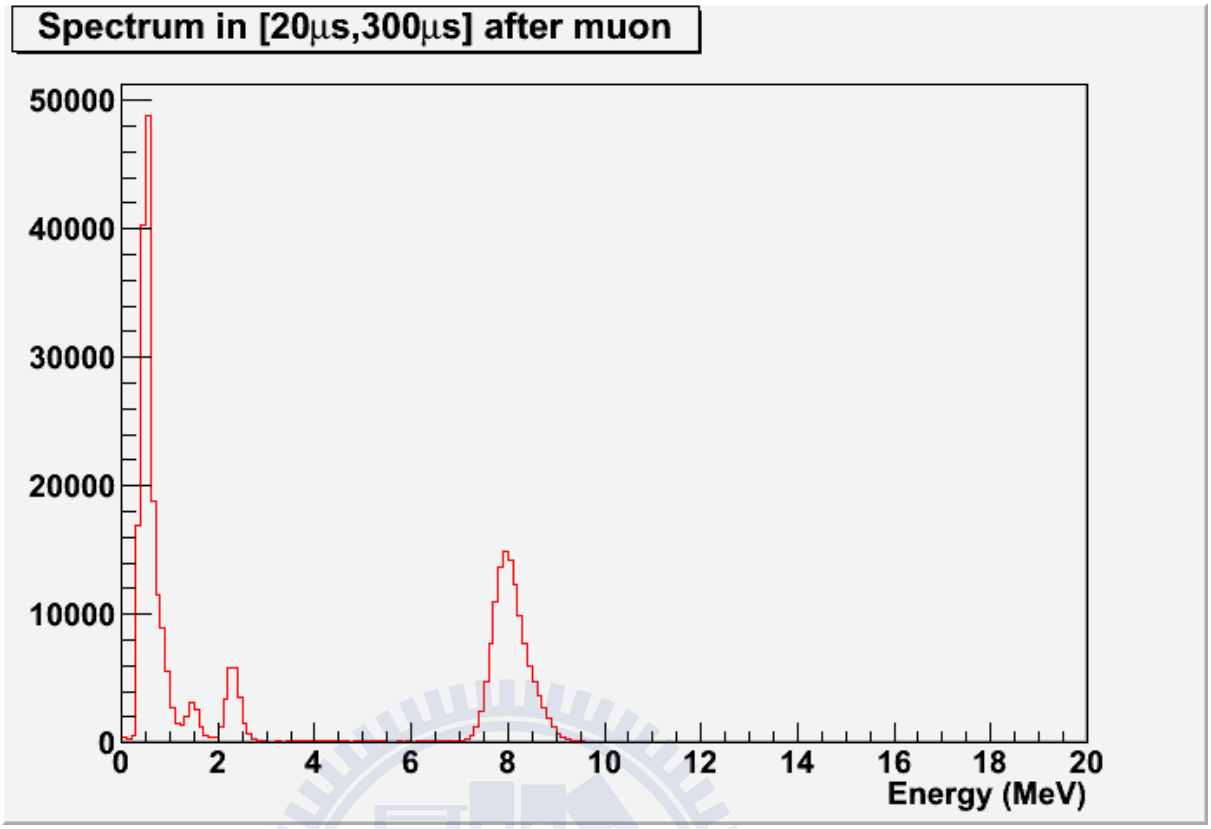

Figure 3.3: The energy spectrum of DYB AD1 in signal time window.

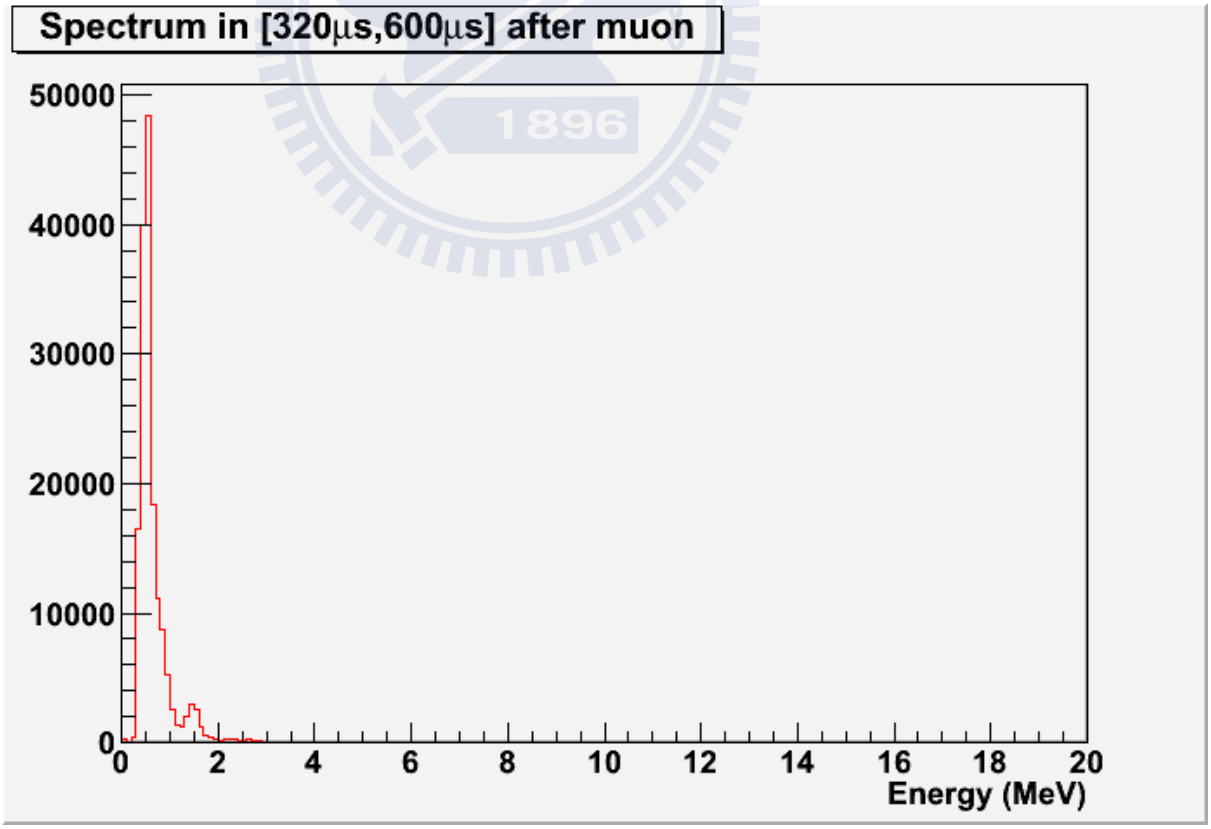

Figure 3.4: The energy spectrum of DYB AD1 in background time window.

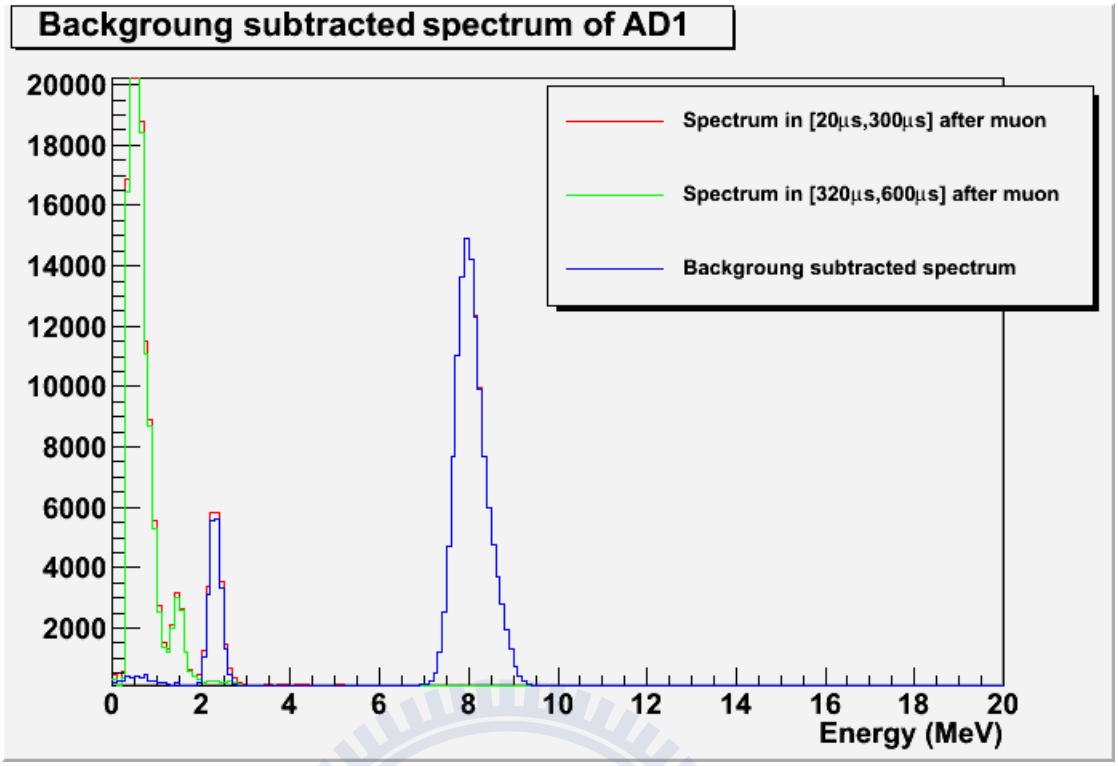

Figure 3.5: The spallation neutron energy spectrum of DYB AD1 with a fiducial cut of radius and height less than 700 mm. The peak around 2 MeV is neutron captured by hydrogen and the peak around 8 MeV is neutron captured by Gd. Red histogram indicates the energy spectrum for total events before background subtraction. Green histogram indicates the energy spectrum in background time window, and the blue histogram shows the energy spectrum after the background subtraction.

The integrated energy range is 3 sigma around the peak. Figure 3.6 to Figure 3.17 show the mean and the sigma of the nH energy peak and the nGd energy peak for each AD separately.

3.3.1 Cut Selection

The ratio $R_{\text{H-Gd}}$ is affected by three cuts, which are fiducial cut (or vertex cut), energy cut, and timing cut. The fiducial cut (F in short) involves two parameters, vertex Z and R ($= \sqrt{X^2 + Y^2}$). Figure 3.18 shows the ratio $R_{\text{H-Gd}}$ with various ranges of fiducial cut for all ADs. The energy cut (E in short) determines the range of the Gd-capture peak and the H-capture peak. We adjusted the range of the Gd-capture peak and the H-

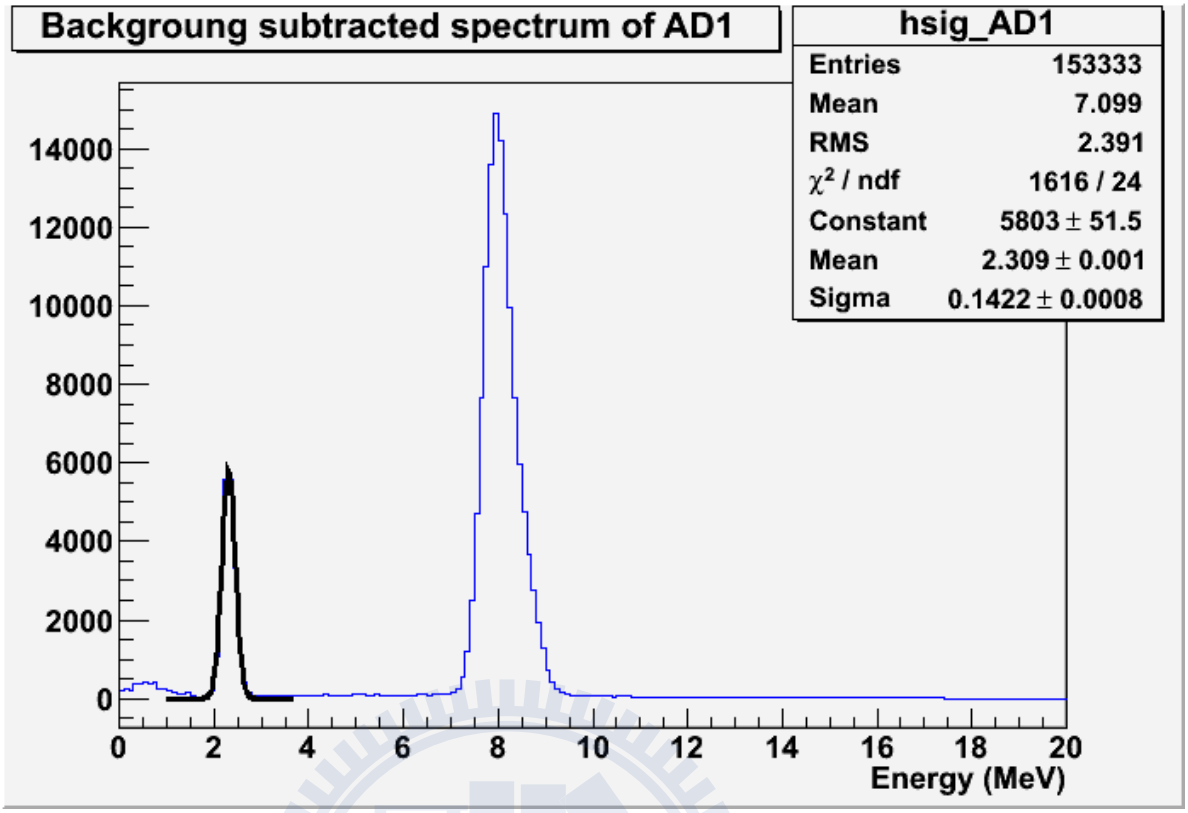

Figure 3.6: The mean and the sigma of the nH energy peak for AD1.

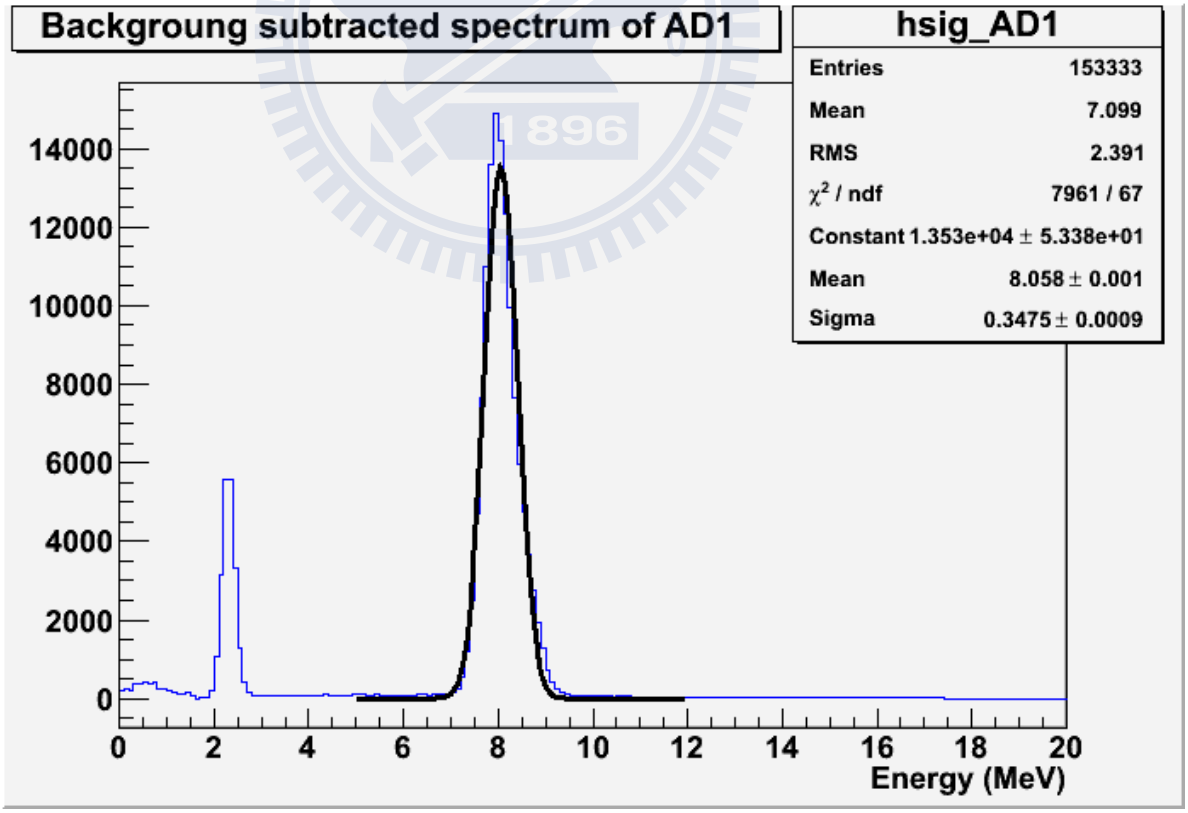

Figure 3.7: The mean and the sigma of the nGd energy peak for AD1.

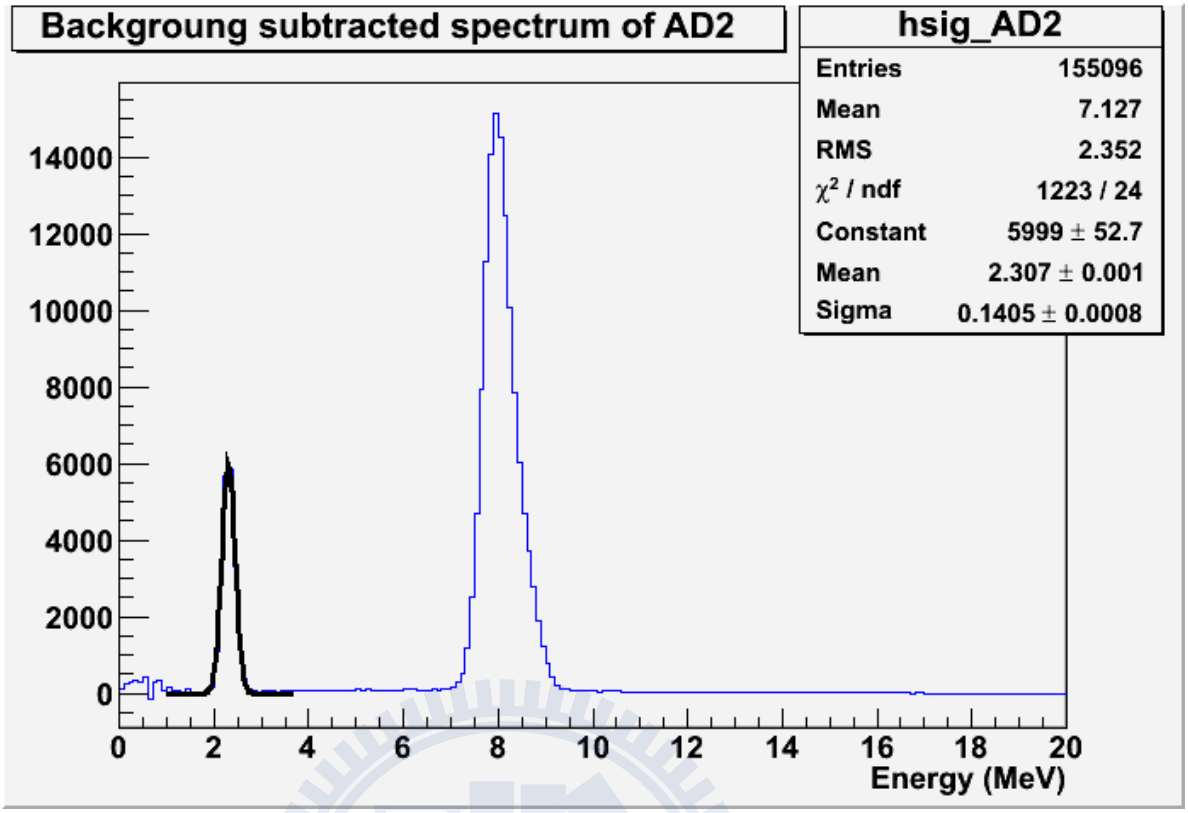

Figure 3.8: The mean and the sigma of the nH energy peak for AD2.

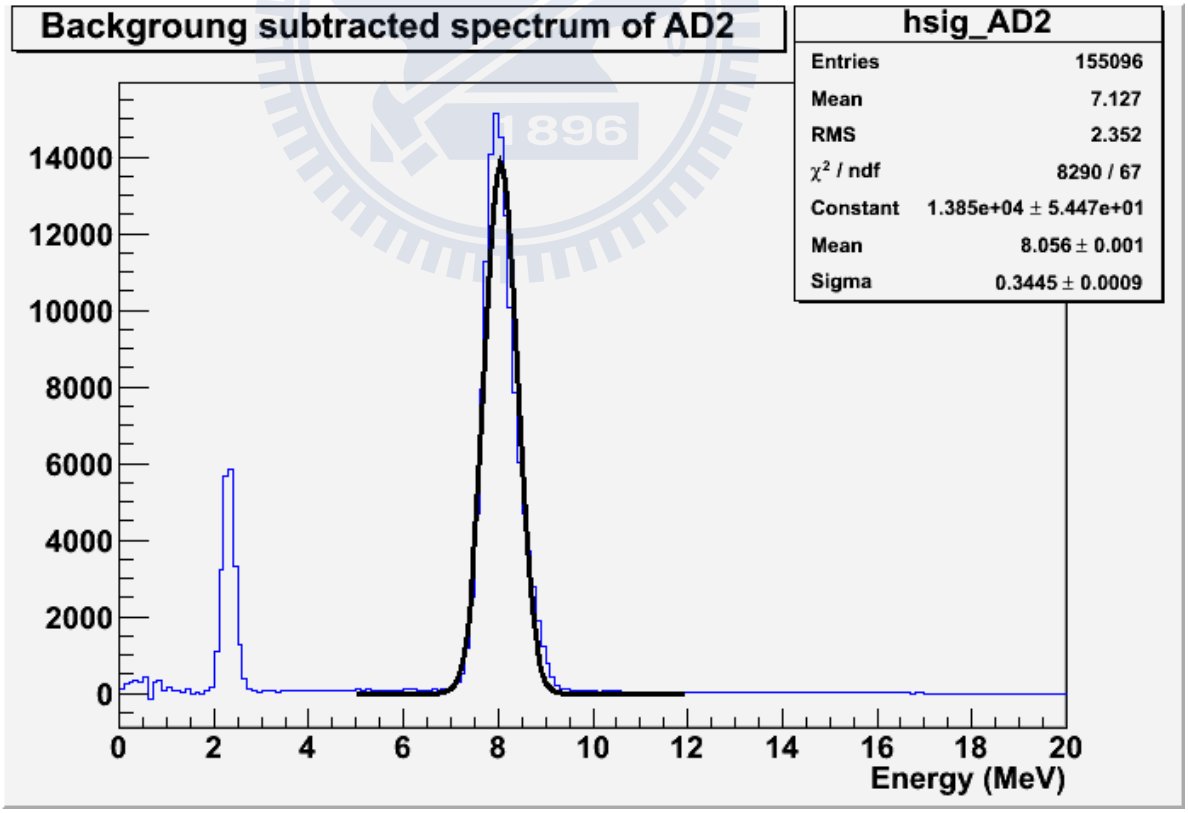

Figure 3.9: The mean and the sigma of the nGd energy peak for AD2.

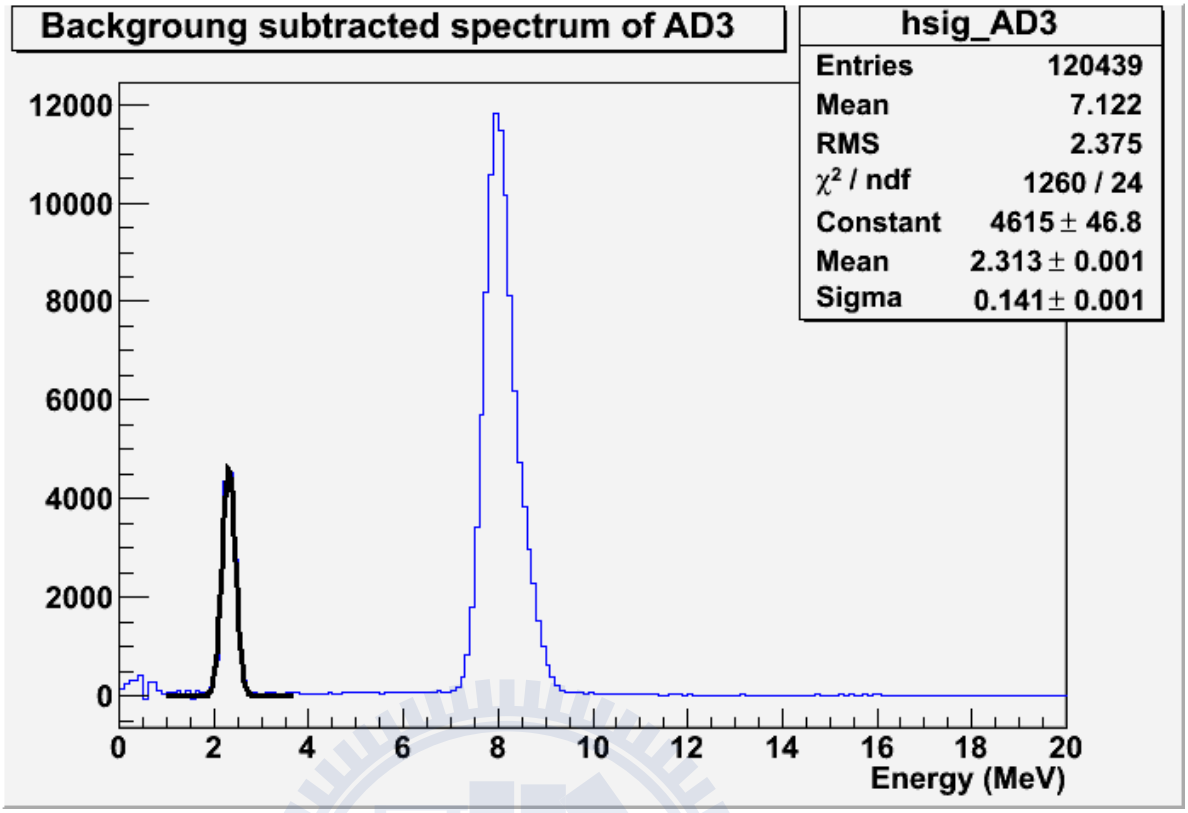

Figure 3.10: The mean and the sigma of the nH energy peak for AD3.

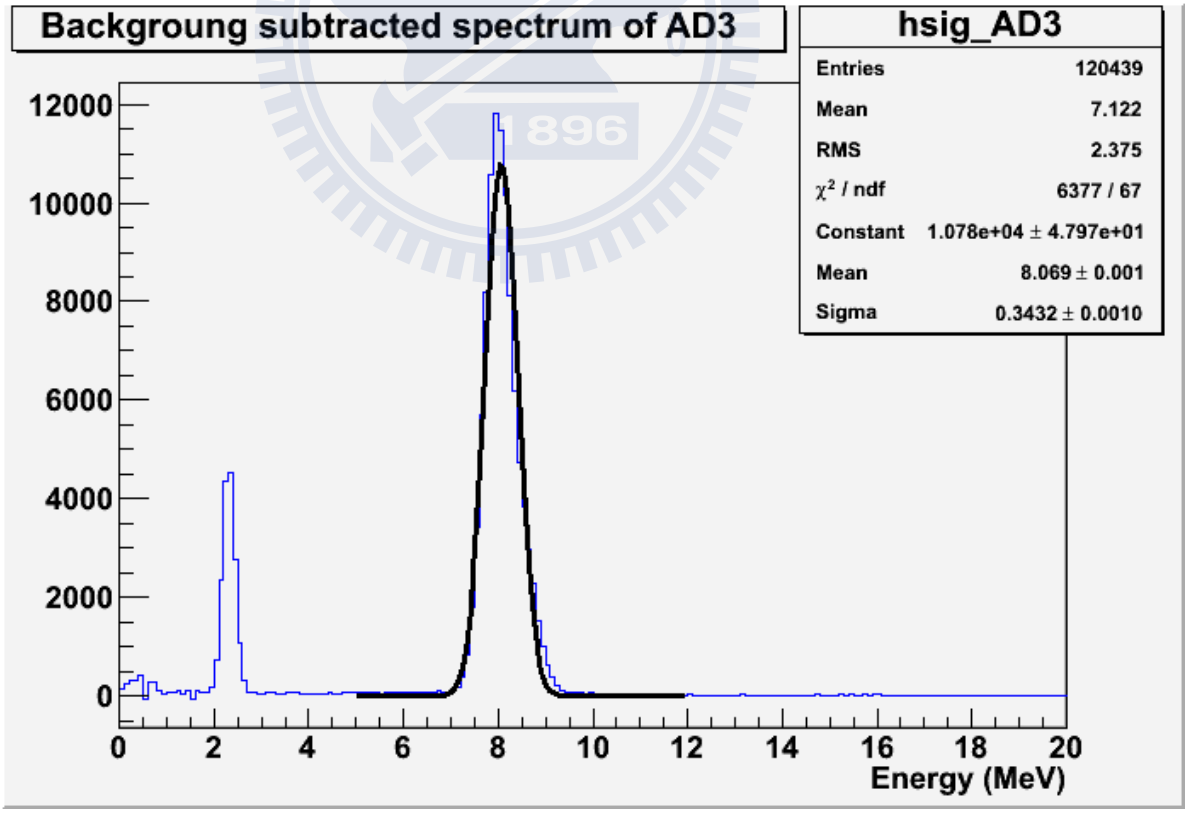

Figure 3.11: The mean and the sigma of the nGd energy peak for AD3.

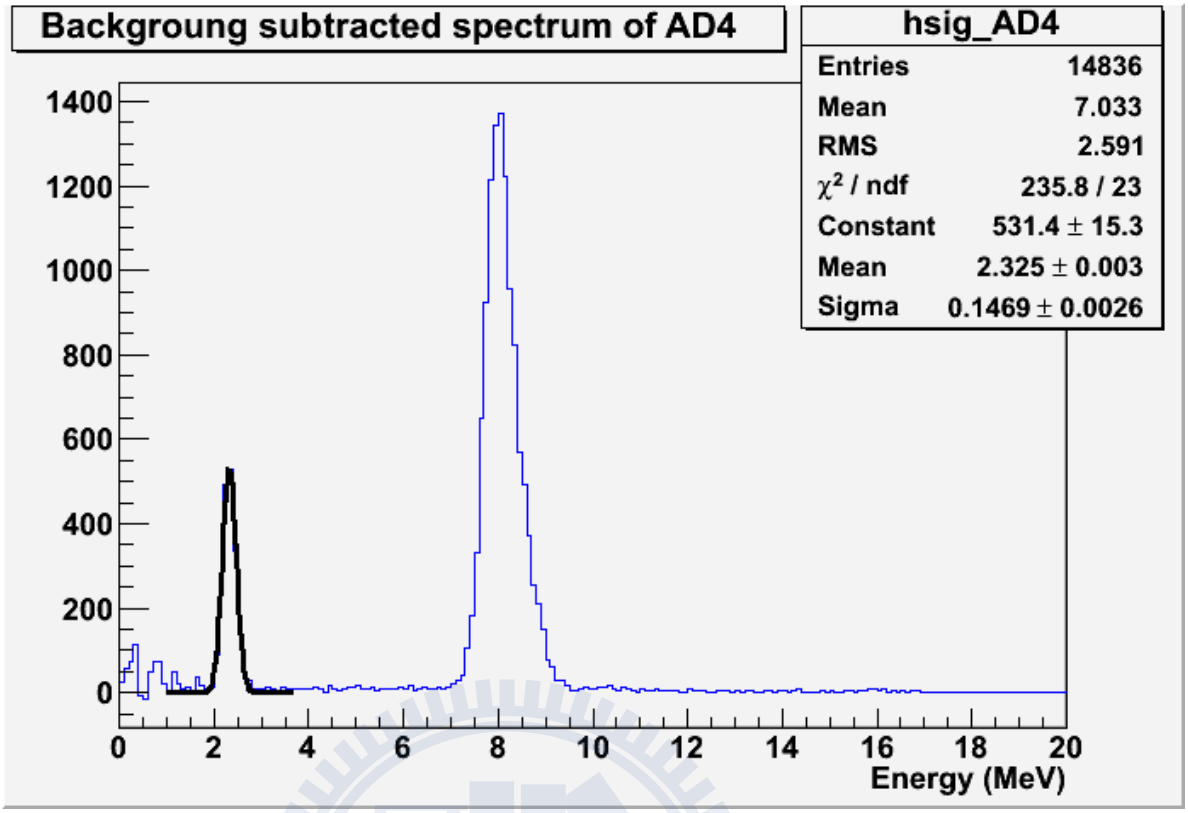

Figure 3.12: The mean and the sigma of the nH energy peak for AD4.

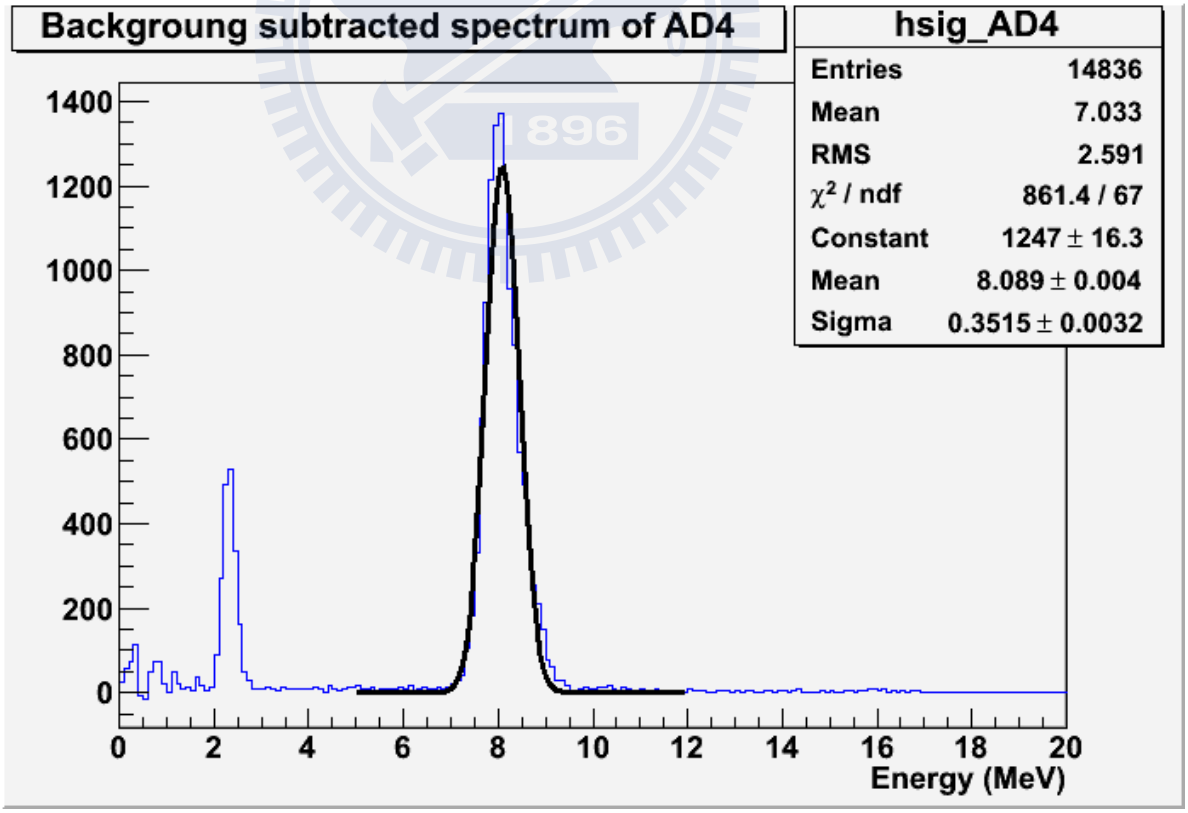

Figure 3.13: The mean and the sigma of the nGd energy peak for AD4.

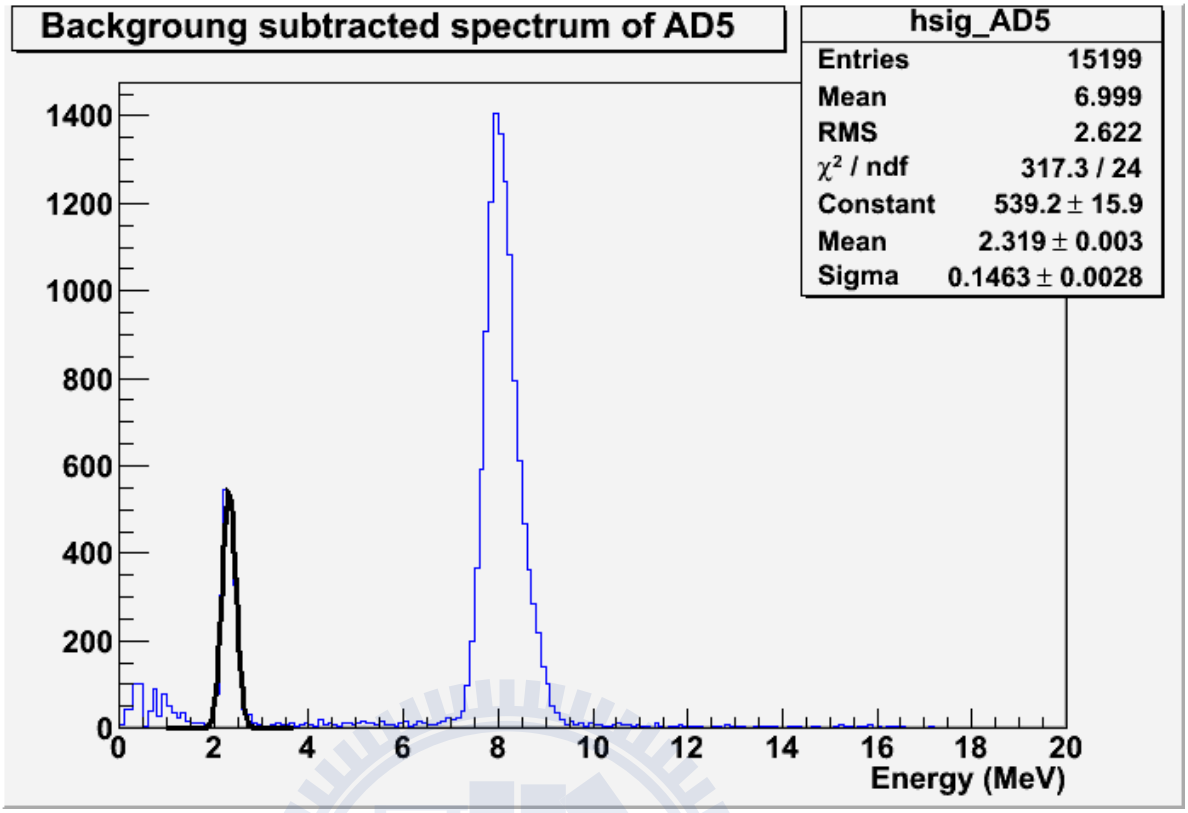

Figure 3.14: The mean and the sigma of the nH energy peak for AD5.

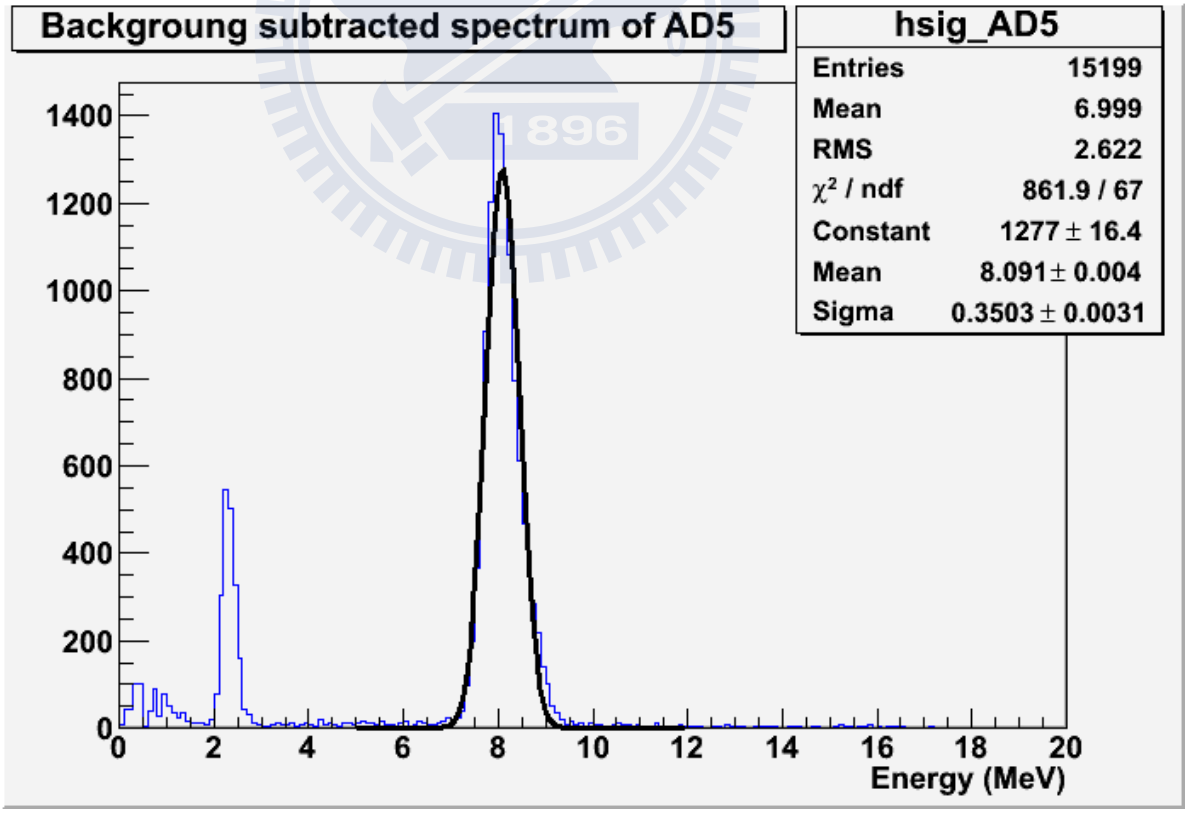

Figure 3.15: The mean and the sigma of the nGd energy peak for AD5.

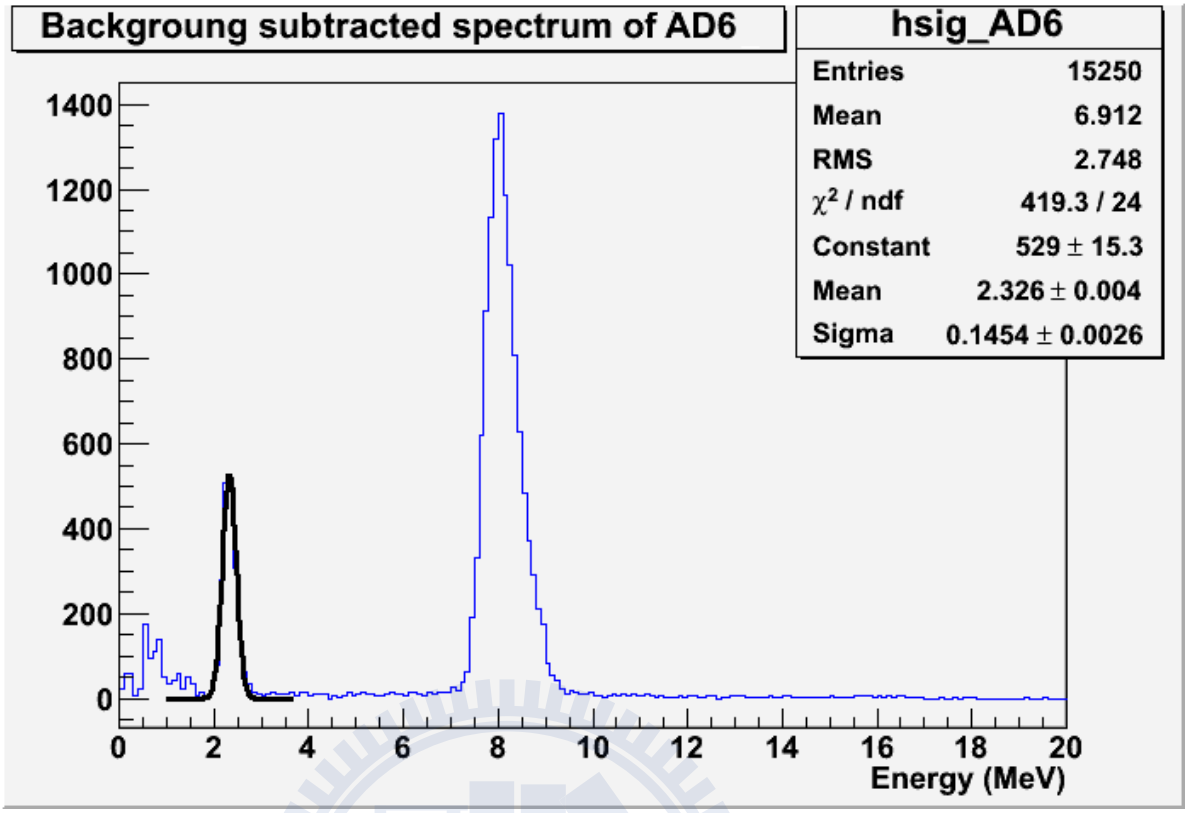

Figure 3.16: The mean and the sigma of the nH energy peak for AD6.

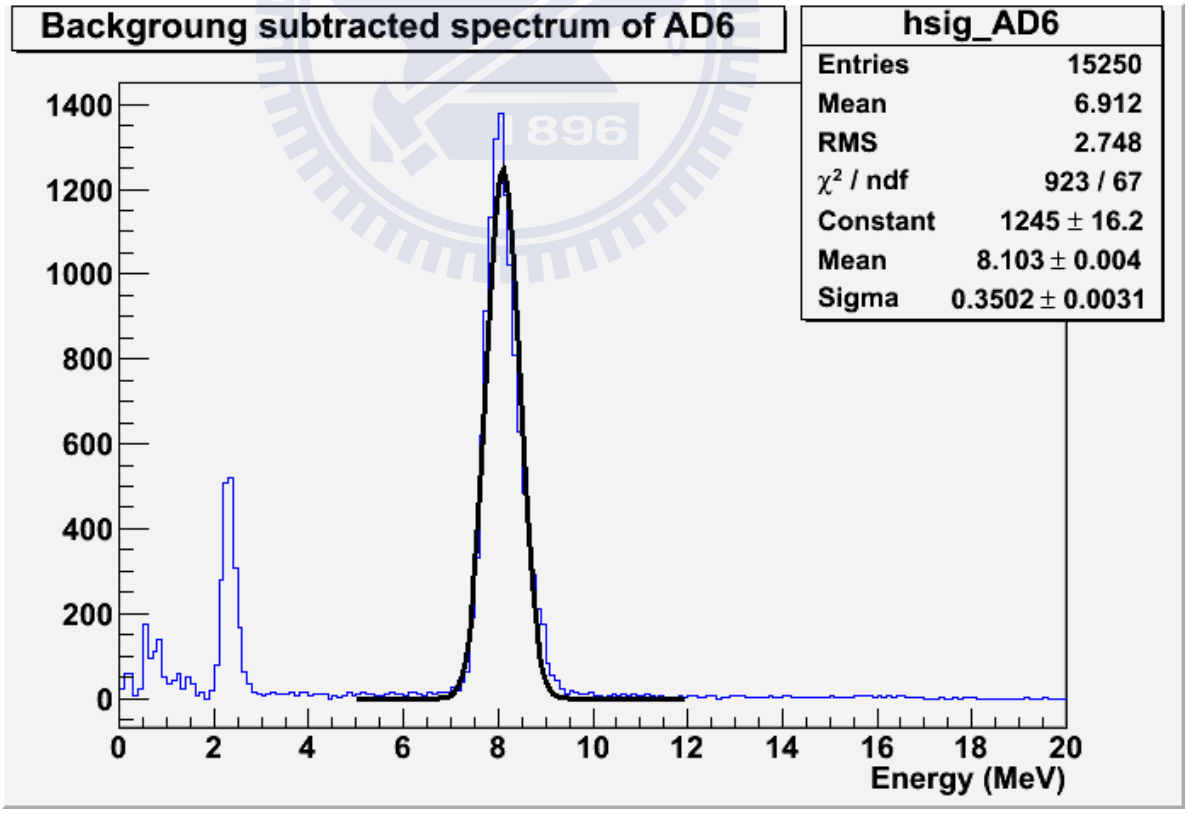

Figure 3.17: The mean and the sigma of the nGd energy peak for AD6.

capture peak simultaneously from 2.5 sigma to 3.5 sigma. The timing cut (T in short) decides the signal time window. The width of the signal time window is kept constant (280 μs) while the beginning of the signal time window is shifted by 1 μs each time and the background time window is moved accordingly.

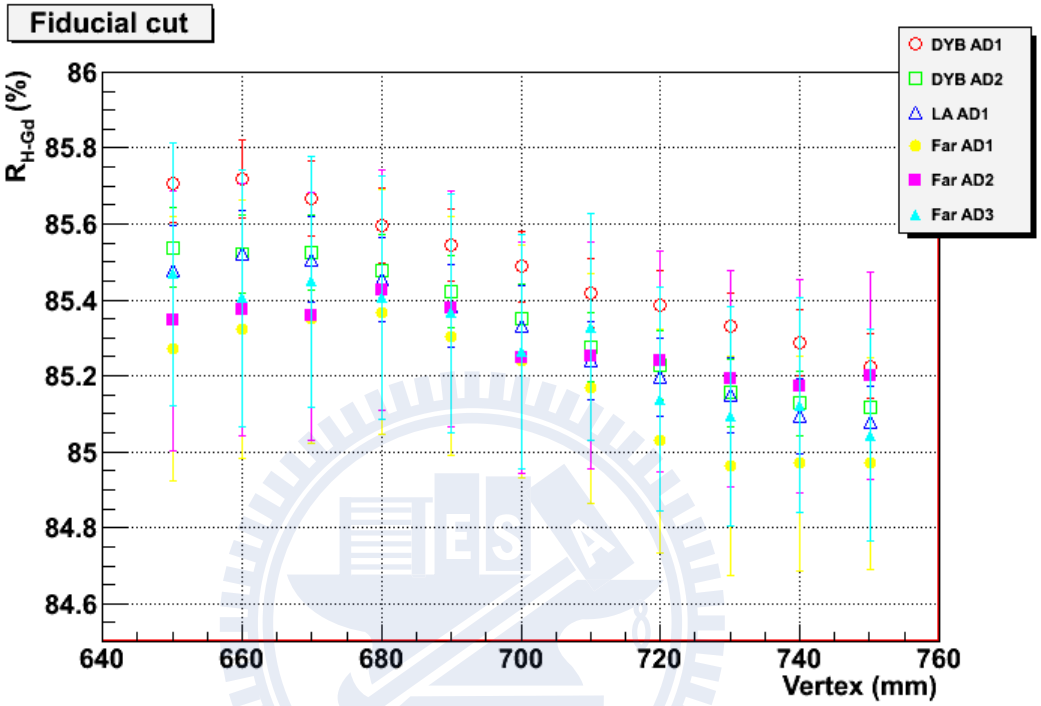

Figure 3.18: The $R_{\text{H-Gd}}$ versus different ranges of fiducial cut. Vertex means $|Z| <$ vertex and R $<$ vertex.

Only one cut out of three is adjusted at once. Namely, when the energy cut is adjusted, the other two cuts are maintained according to the criteria in Section 3.2. We show the results of various energy cuts and timing cuts in Figure 3.19 and Figure 3.20, respectively.

In the plots, the statistical error (σ_{stat}) is calculated by

$$\sigma_{\text{stat}} = \sqrt{\frac{R_{\text{H-Gd}}(1 - R_{\text{H-Gd}})}{N_{\text{total}}}}, \tag{3.2}$$

It is the standard deviation for binomial distribution.

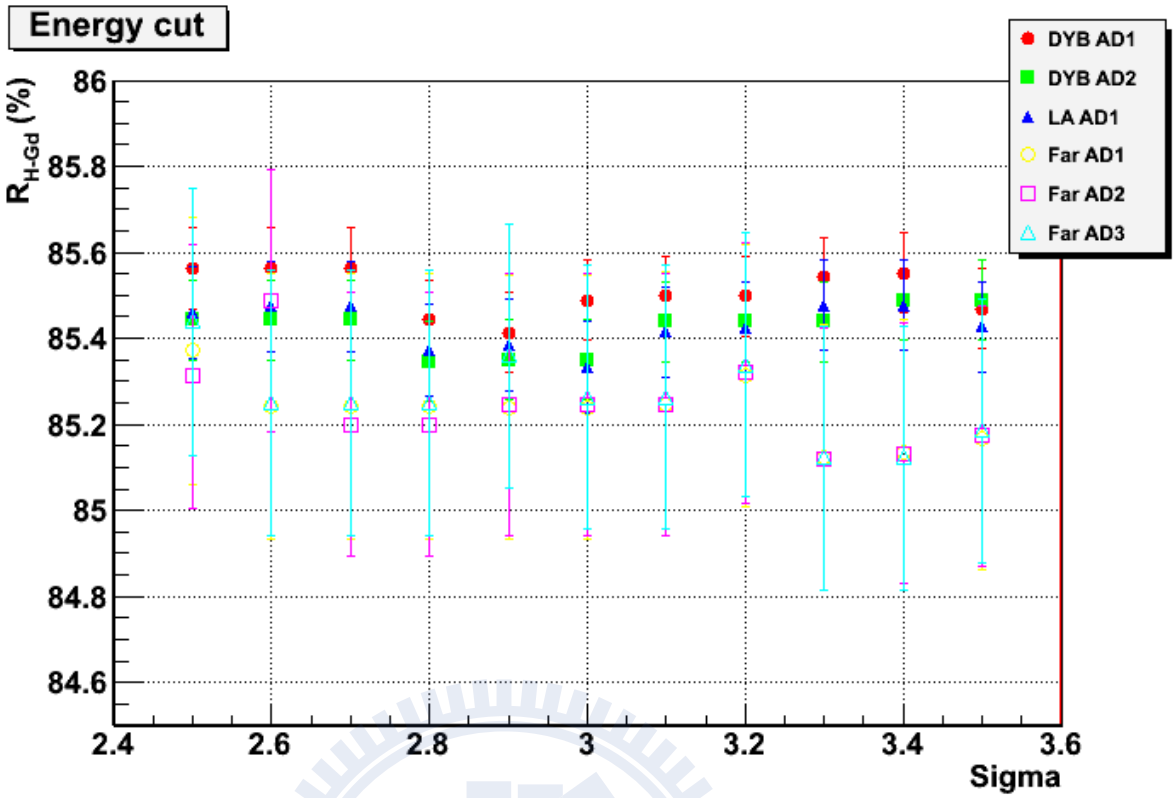

Figure 3.19: The $R_{\text{H-Gd}}$ versus various energy cuts for all ADs.

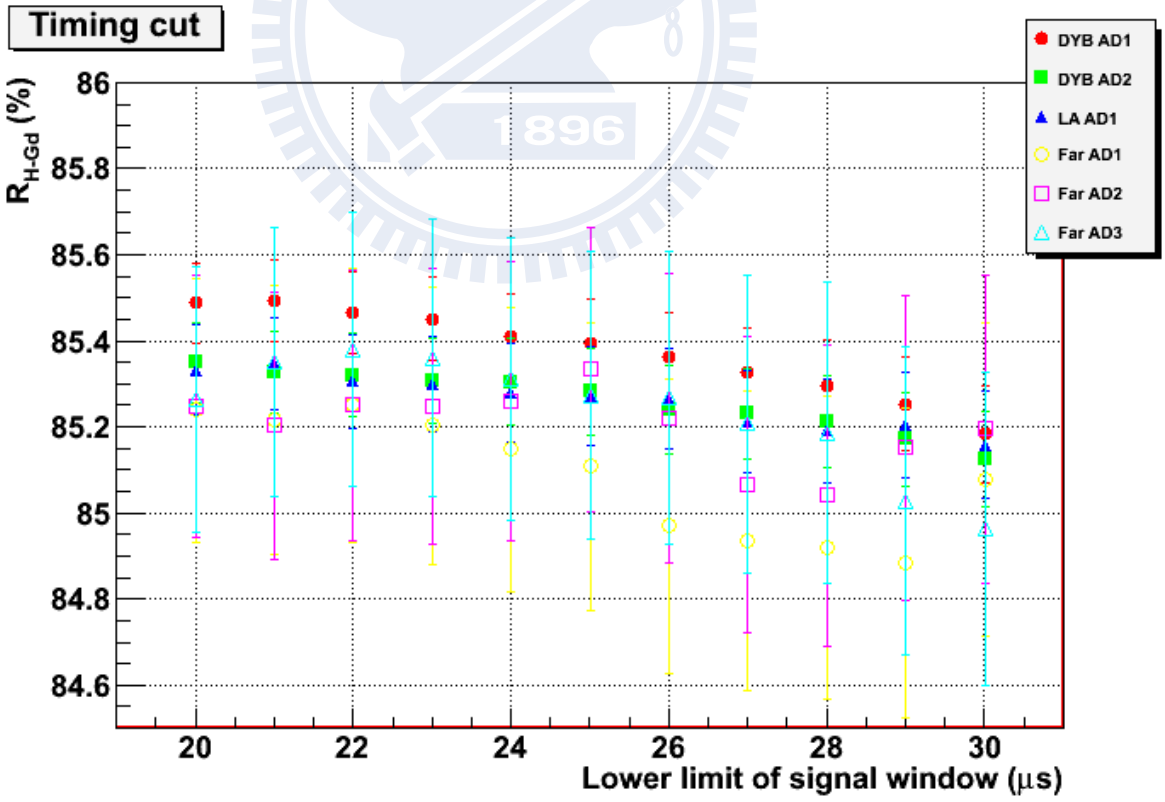

Figure 3.20: The $R_{\text{H-Gd}}$ versus various timing cuts for all ADs.

3.3.2 Cut Efficiency

We have calculated different cut efficiencies by Monte Carlo (MC) method (the data was produced by Yung-Shun Yeh[10]). For all cut selections, we considered the efficiency of nGd and of nH separately.

The cut efficiency of the fiducial cut (ϵ_{FnGd} and ϵ_{FnH}) are defined as follows,

$$\epsilon_{FnGd} = \frac{\text{Number of nGd with fiducial cut}}{\text{Number of nGd in GdLS}} \tag{3.3}$$

and

$$\epsilon_{FnH} = \frac{\text{Number of nH with fiducial cut}}{\text{Number of nH in GdLS}}. \tag{3.4}$$

Similarly, the other cut efficiency can be defined as follows：

$$\epsilon_{TnGd} = \frac{\text{Number of nGd with timing cut in GdLS}}{\text{Number of nGd in GdLS}} \tag{3.5}$$

$$\epsilon_{TnH} = \frac{\text{Number of nH with timing cut in GdLS}}{\text{Number of nH in GdLS}} \tag{3.6}$$

$$\epsilon_{EnGd} = \frac{\text{Number of nGd with energy cut in GdLS}}{\text{Number of nGd in GdLS}} \tag{3.7}$$

$$\epsilon_{EnH} = \frac{\text{Number of nH with energy cut in GdLS}}{\text{Number of nH in GdLS}}. \tag{3.8}$$

Figure 3.21 to Figure 3.26 show the results of various cut efficiencies.

Then, we define the new ratio $R'_{\text{H-Gd}}$ with cut efficiency ϵ_{Gd} ($= \epsilon_{FnGd} \times \epsilon_{TnGd} \times \epsilon_{EnGd}$) and ϵ_H ($= \epsilon_{FnH} \times \epsilon_{TnH} \times \epsilon_{EnH}$) instead of the $R_{\text{H-Gd}}$ as

$$R'_{\text{H-Gd}} = \frac{\frac{N_{\text{Gd}}}{\epsilon_{Gd}}}{\frac{N_{\text{Gd}}}{\epsilon_{Gd}} + \frac{N_{\text{H}}}{\epsilon_H}}. \tag{3.9}$$

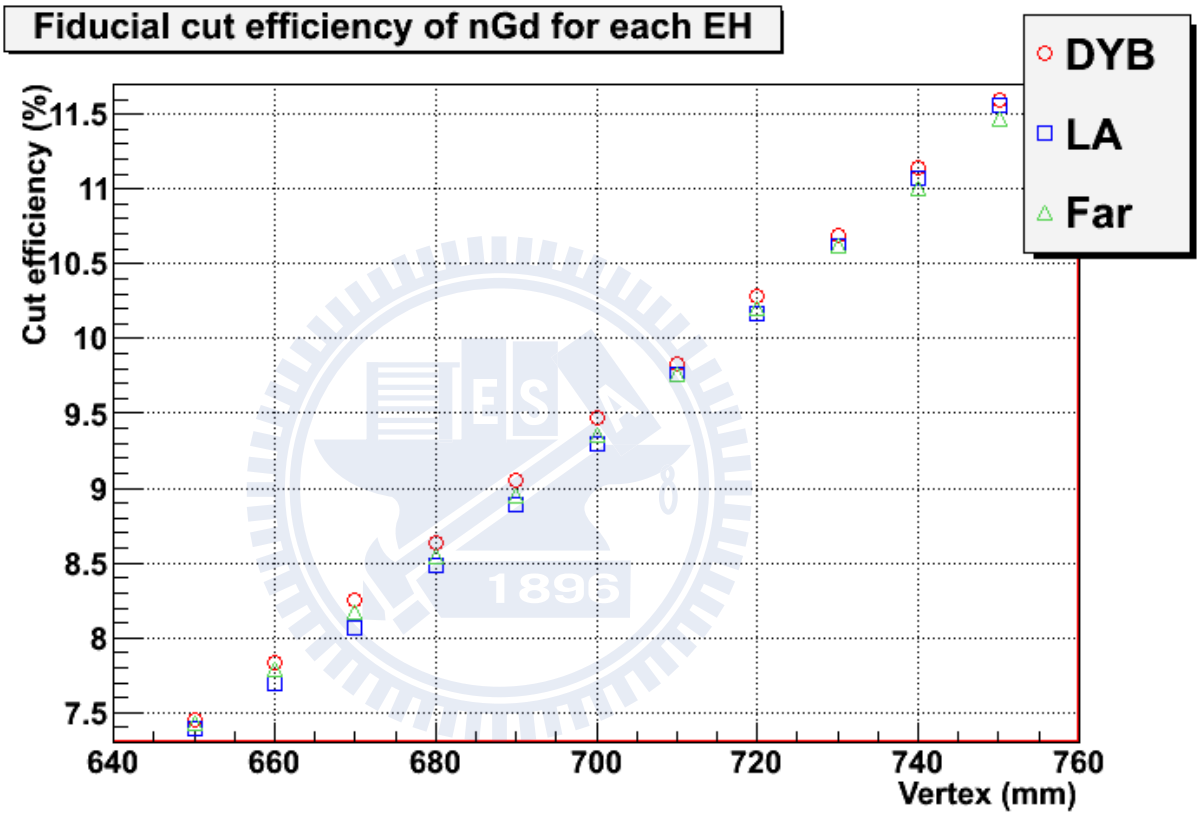

Figure 3.21: The ϵ_{FnGd} versus various fiducial cuts.

We also redefine the σ_{stat} with cut efficiency as

$$\sigma'_{\text{stat}} = R'_{\text{H-Gd}} \left(R'_{\text{H-Gd}} - 1\right) \sqrt{\frac{1}{N_{\text{H}}} + \frac{1}{N_{\text{Gd}}}}. \tag{3.10}$$

The derivation of σ'_{stat} is shown in Appendix A. Figure 3.27 to Figure 3.29 and Figure 3.1 to Figure 3.3 show results of $R'_{\text{H-Gd}}$ and σ'_{stat}.

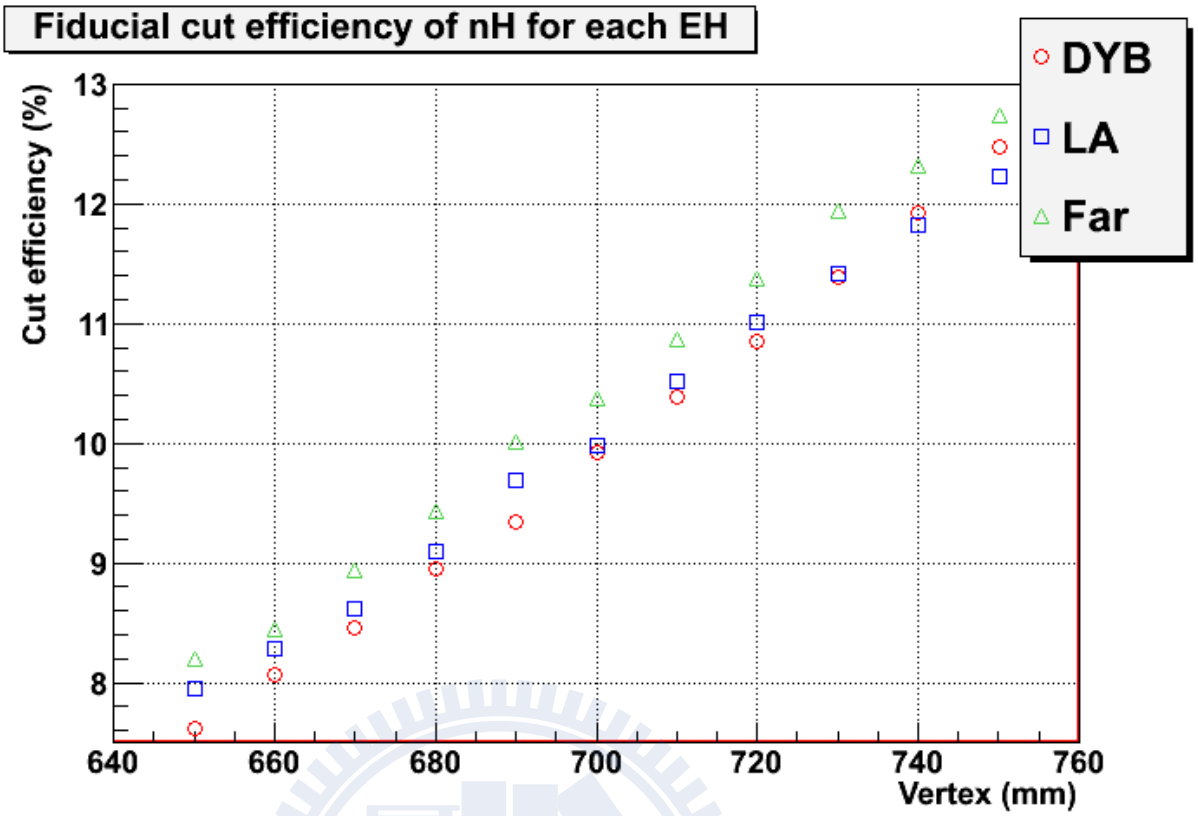

Figure 3.22: The ϵ_{FnH} versus various fiducial cuts.

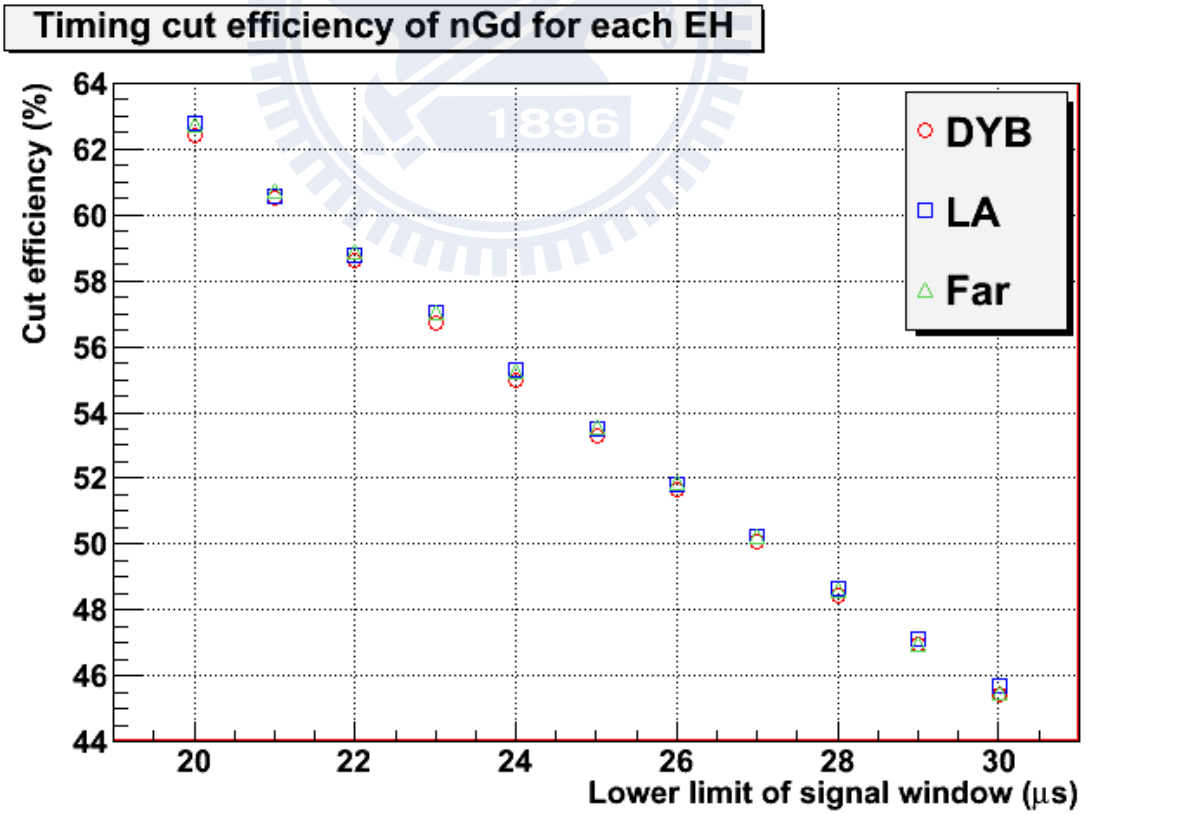

Figure 3.23: The ϵ_{TnGd} versus various timing cuts.

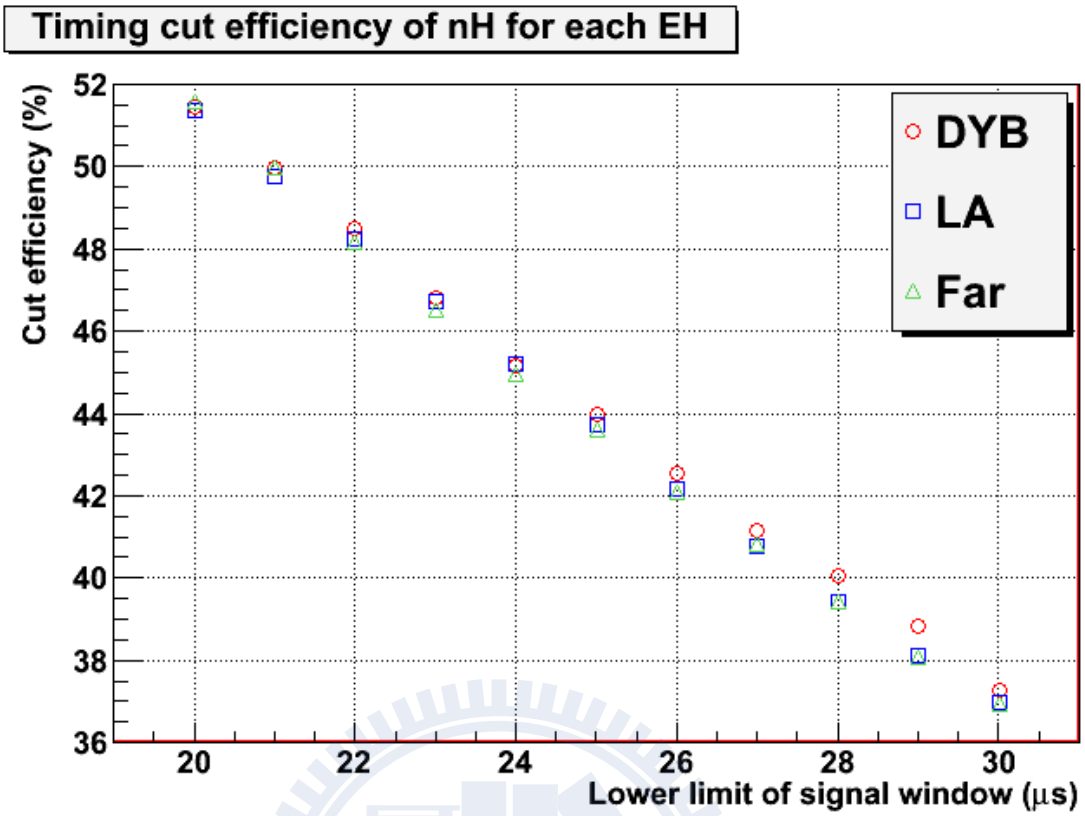

Figure 3.24: The ϵ_{TnH} versus various timing cuts.

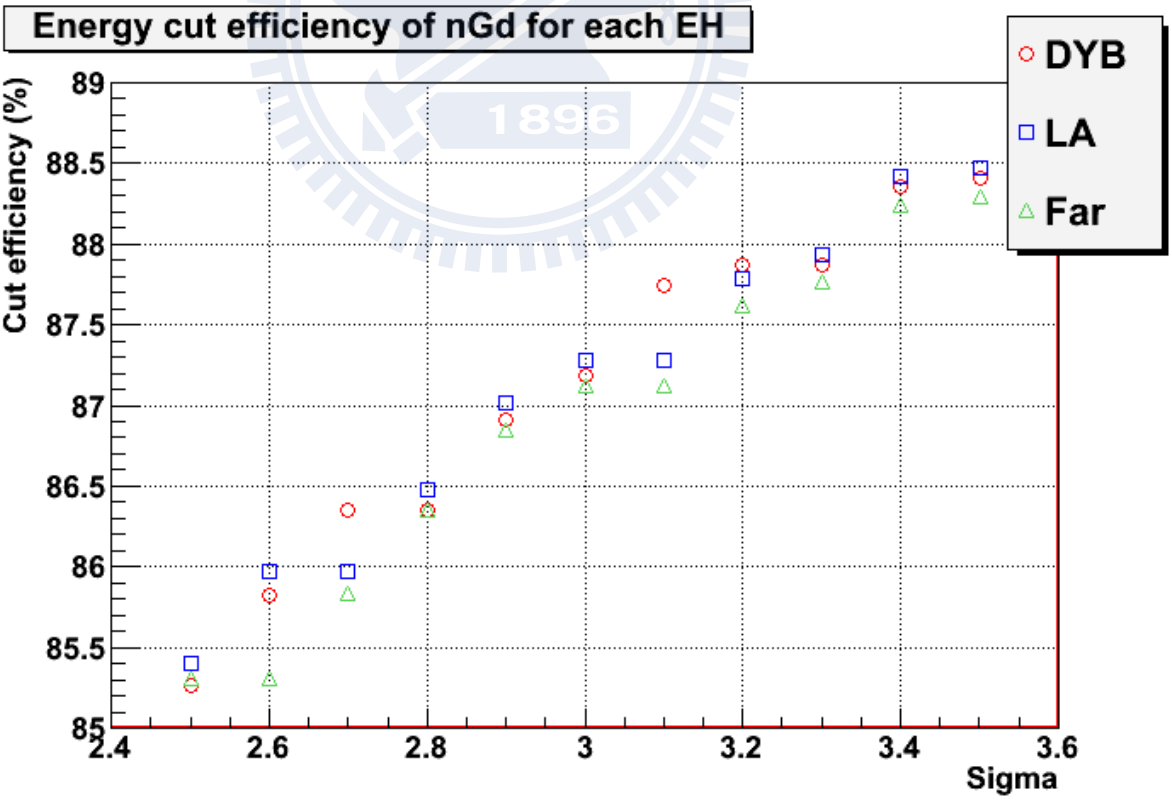

Figure 3.25: The ϵ_{EnGd} versus various energy cuts.

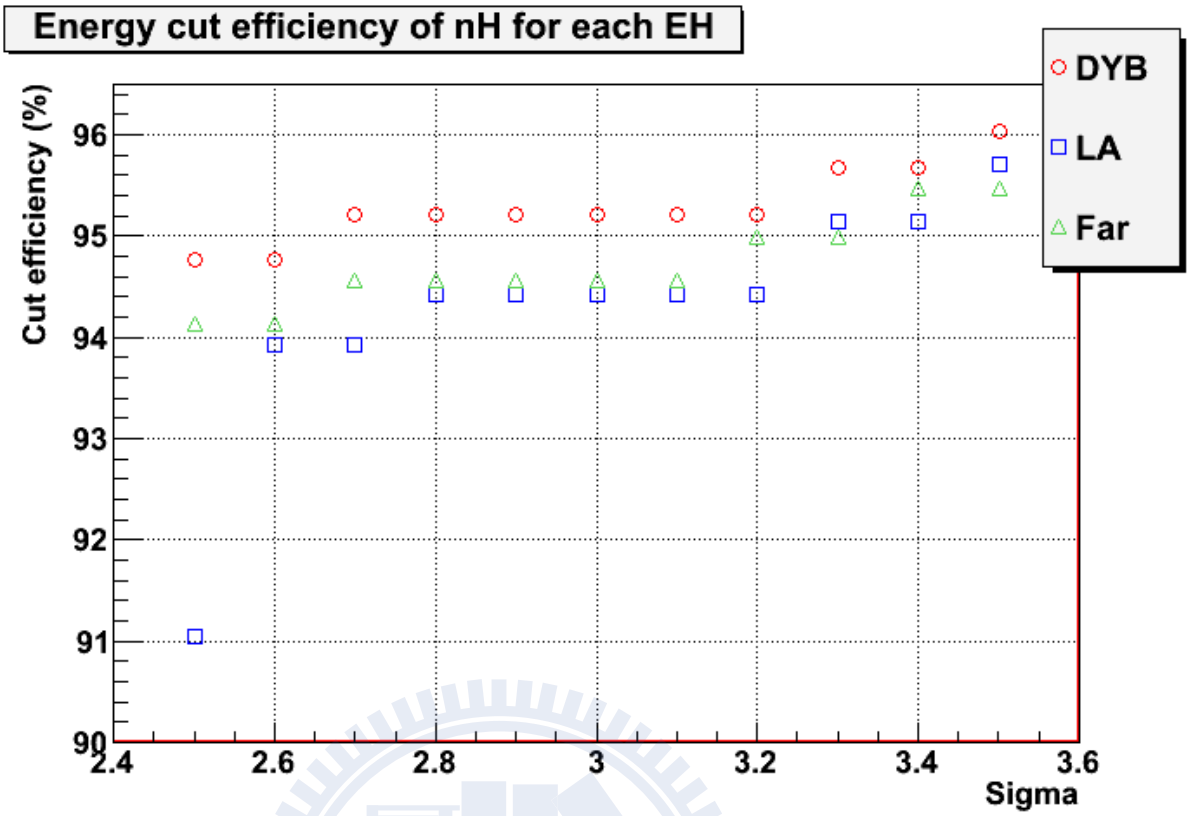

Figure 3.26: The ϵ_{EnH} versus various energy cuts.

E	AD1		AD2		AD3		AD4		AD5		AD6	
(Sigma)	R' (%)	σ' (%)	R' (%)	σ' (%)	R' (%)	σ' (%)	R' (%)	σ' (%)	R' (%)	σ' (%)	R' (%)	σ' (%)
2.5	85.05	0.1	84.93	0.1	84.61	0.11	85.44	0.31	85.39	0.31	85.51	0.31
2.6	84.97	0.1	84.84	0.1	84.94	0.11	85.32	0.31	85.56	0.3	85.32	0.31
2.7	84.95	0.1	84.83	0.1	84.94	0.11	85.3	0.31	85.25	0.31	85.31	0.31
2.8	84.83	0.1	84.73	0.1	84.83	0.11	85.22	0.31	85.18	0.31	85.23	0.31
2.9	84.71	0.1	84.65	0.1	84.76	0.11	85.15	0.31	85.15	0.31	85.27	0.31
3	84.75	0.1	84.6	0.1	84.67	0.11	85.11	0.31	85.11	0.31	85.13	0.31
3.1	84.68	0.1	84.61	0.1	84.76	0.11	85.11	0.31	85.11	0.31	85.13	0.31
3.2	84.66	0.1	84.6	0.1	84.69	0.11	85.17	0.31	85.17	0.31	85.19	0.31
3.3	84.77	0.1	84.66	0.1	84.82	0.11	84.95	0.31	84.95	0.31	84.95	0.31
3.4	84.7	0.1	84.64	0.1	84.75	0.11	84.96	0.31	84.96	0.31	84.95	0.31
3.5	84.66	0.1	84.68	0.1	84.77	0.11	84.99	0.31	84.99	0.31	85	0.31

Table 3.1: The $R'_{\text{H-Gd}}$ and σ'_{stat} of energy cuts for each AD.

3.3.3 Ratio, Statistical Error and Systematical Error for Each AD

We already obtained 66 sets of the $R'_{\text{H-Gd}}$ and the σ'_{stat} for each AD. Then, we use 11 sets of data for each cut selections for each AD to get systematical error for energy cut, fiducial cut, and timing cut.

At first, we calculate the mean of the 11 sets of the $R'_{\text{H-Gd}}$ for each cut selections,

F	AD1		AD2		AD3		AD4		AD5		AD6	
(mm)	R' (%)	σ' (%)	R' (%)	σ' (%)	R' (%)	σ' (%)	R' (%)	σ' (%)	R' (%)	σ' (%)	R' (%)	σ' (%)
650	84.67	0.11	84.49	0.11	84.84	0.12	85.09	0.35	85.16	0.35	85.29	0.35
660	84.77	0.11	84.56	0.11	84.9	0.12	84.9	0.35	84.95	0.34	84.99	0.35
670	84.66	0.11	84.51	0.11	84.78	0.12	85.05	0.34	85.06	0.33	85.15	0.34
680	84.71	0.1	84.59	0.1	84.79	0.11	85.18	0.33	85.24	0.32	85.22	0.33
690	84.61	0.1	84.47	0.1	84.92	0.11	85.29	0.32	85.36	0.31	85.35	0.32
700	84.75	0.1	84.6	0.1	84.67	0.11	85.11	0.31	85.11	0.31	85.13	0.31
710	84.79	0.09	84.64	0.09	84.64	0.11	85.08	0.3	85.17	0.3	85.24	0.3
720	84.73	0.09	84.57	0.09	84.66	0.1	84.96	0.3	85.17	0.29	85.07	0.3
730	84.8	0.09	84.62	0.09	84.5	0.1	85.01	0.29	85.24	0.28	85.14	0.29
740	84.82	0.09	84.66	0.09	84.36	0.1	84.96	0.28	85.16	0.28	85.11	0.28
750	84.82	0.09	84.71	0.09	84.22	0.1	84.85	0.28	85.09	0.28	84.93	0.28

Table 3.2: The $R'_{\text{H-Gd}}$ and σ'_{stat} of fiducial cuts for each AD.

T	AD1		AD2		AD3		AD4		AD5		AD6	
(μs)	R' (%)	σ' (%)	R' (%)	σ' (%)	R' (%)	σ' (%)	R' (%)	σ' (%)	R' (%)	σ' (%)	R' (%)	σ' (%)
[20,300]	84.75	0.1	84.6	0.1	84.67	0.11	85.11	0.31	85.11	0.31	85.13	0.31
[21,301]	84.77	0.1	84.6	0.1	84.74	0.11	85.09	0.31	85.08	0.31	85.23	0.31
[22,302]	84.77	0.1	84.62	0.1	84.69	0.11	85.04	0.32	85.04	0.32	85.18	0.32
[23,303]	84.72	0.1	84.57	0.1	84.66	0.12	84.97	0.33	85.01	0.32	85.13	0.33
[24,304]	84.62	0.1	84.51	0.1	84.61	0.12	84.87	0.33	84.99	0.33	85.04	0.33
[25,305]	84.66	0.11	84.54	0.11	84.6	0.12	84.85	0.34	85.07	0.33	85.01	0.34
[26,306]	84.6	0.11	84.47	0.11	84.53	0.12	84.66	0.35	84.92	0.34	84.97	0.34
[27,307]	84.54	0.11	84.44	0.11	84.45	0.12	84.64	0.35	84.77	0.35	84.92	0.35
[28,308]	84.59	0.11	84.5	0.11	84.4	0.13	84.62	0.36	84.74	0.36	84.89	0.36
[29,309]	84.54	0.11	84.46	0.11	84.4	0.13	84.56	0.37	84.84	0.36	84.71	0.36
[30,310]	84.36	0.12	84.3	0.12	84.35	0.13	84.78	0.37	84.9	0.37	84.67	0.37

Table 3.3: The $R'_{\text{H-Gd}}$ and σ'_{stat} of timing cuts for each AD.

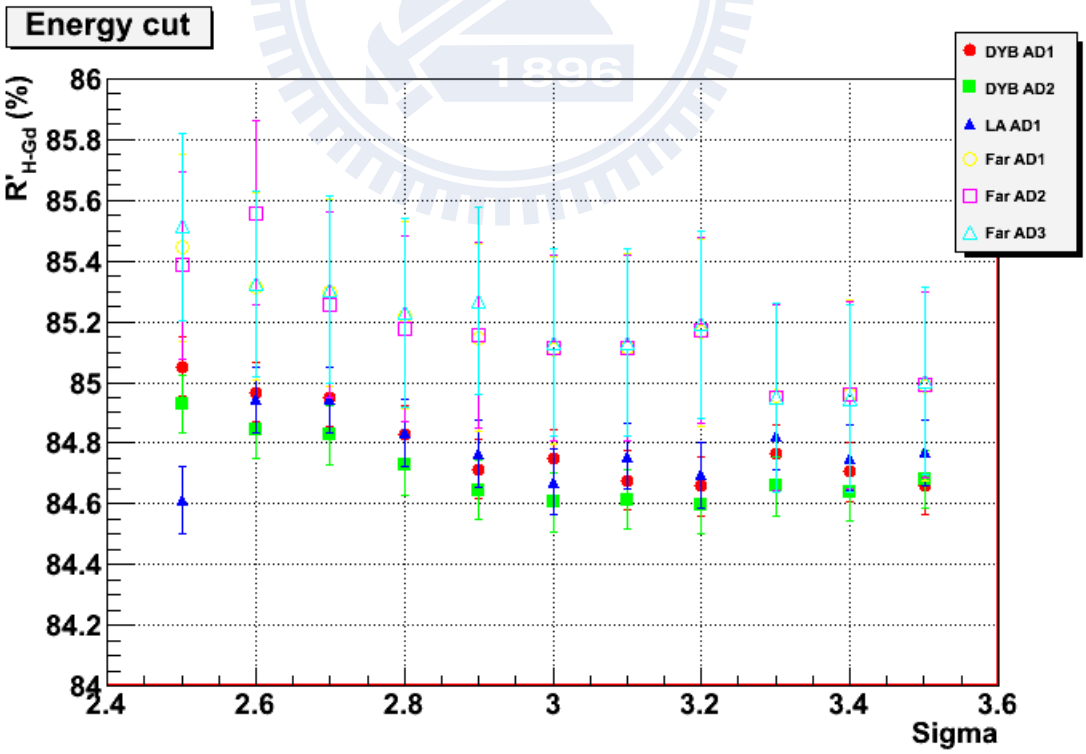

Figure 3.27: The $R'_{\text{H-Gd}}$ versus various energy cuts.

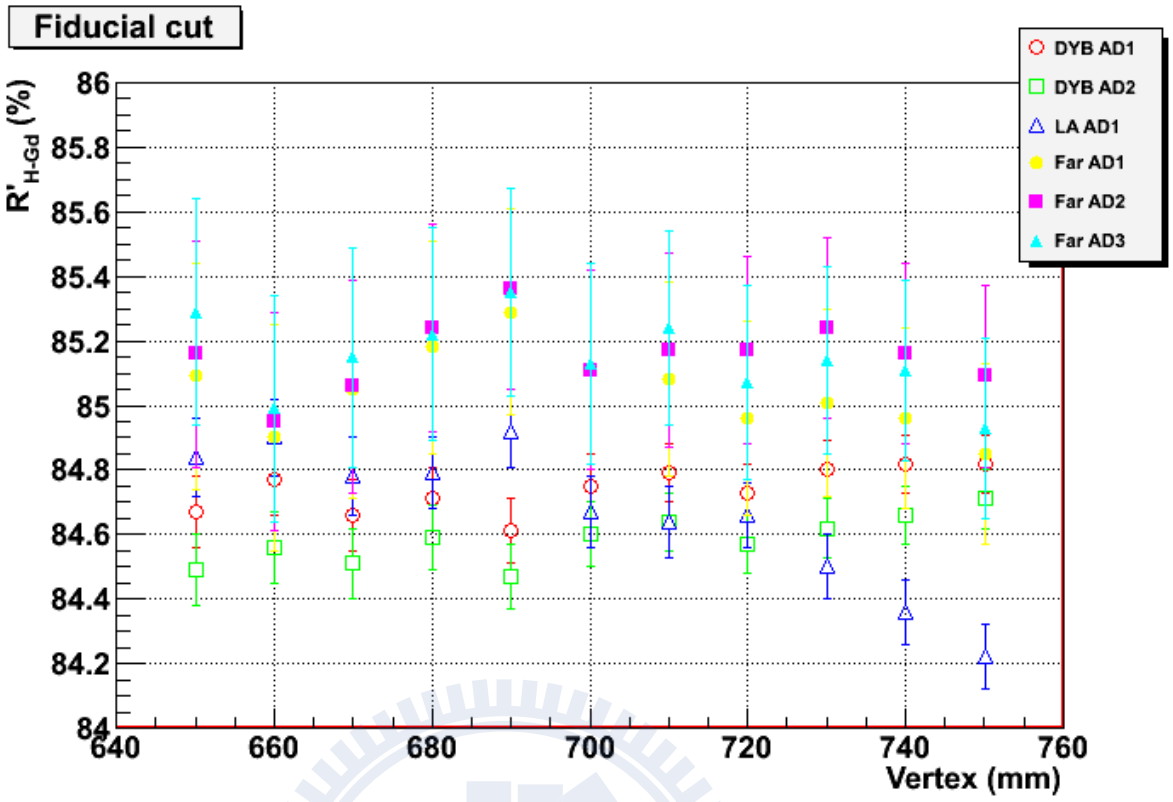

Figure 3.28: The $R'_{\text{H-Gd}}$ versus various fiducial cuts.

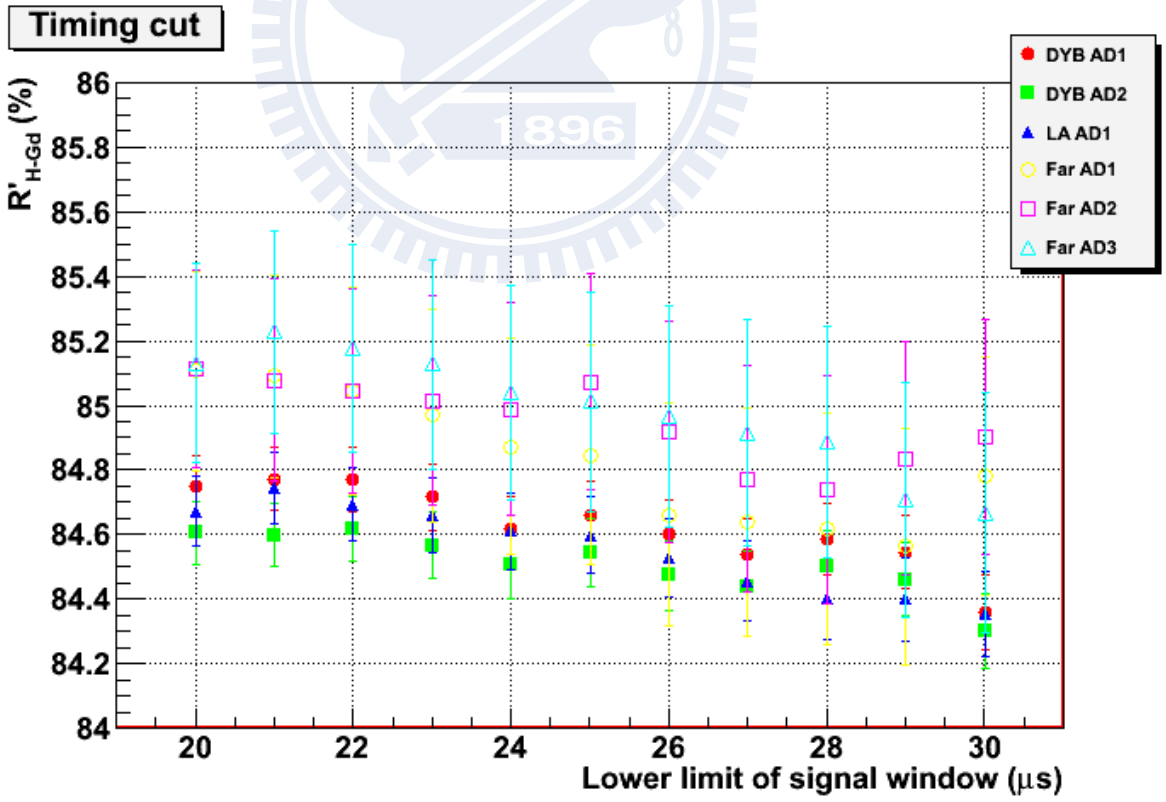

Figure 3.29: The $R'_{\text{H-Gd}}$ versus various timing cuts.

called R'_{mean}. Then we define the σ_{sysF}, σ_{sysE}, and σ_{sysT} as

$$\sigma_{\text{sys}} = \sqrt{\frac{1}{10}\sum_{i=1}^{11}\left(R'_{\text{H-Gd}} - R'_{\text{mean}}\right)^2}, \tag{3.11}$$

and define the $\sigma_{\text{syst}} = \sqrt{(\sigma_{\text{sysF}})^2 + (\sigma_{\text{sysE}})^2 + (\sigma_{\text{sysT}})^2}$. Table 3.4 shows the result.

	AD1	**AD2**	**AD3**	**AD4**	**AD5**	**AD6**
σ_{sysF} **(%)**	0.07	0.07	0.22	0.13	0.11	0.12
σ_{sysE} **(%)**	0.14	0.11	0.1	0.16	0.18	0.17
σ_{sysT} **(%)**	0.12	0.09	0.14	0.2	0.13	0.18
σ_{syst} **(%)**	0.2	0.16	0.28	0.29	0.25	0.28

Table 3.4: The σ_{sysF}, σ_{sysE}, σ_{sysT}, and σ_{syst} for each AD.

The ratio and the statistical error for each AD are $R'_{\text{H-Gd}}$ and σ'_{stat} which satisfy the criteria in Section 3.2.

Chapter 4

Conclusion

We analyzed and calculated the H-Gd ratio, cut efficiency, statistical error, and systematical error for 6 ADs in Daya Bay experiment. The following is the results of the H-Gd ratio (R)：

$$R_{\text{AD1}} = 84.75\% \pm 0.10\%(\text{stat.}) \pm 0.20\%(\text{syst.}) \tag{4.1}$$

$$R_{\text{AD2}} = 84.60\% \pm 0.10\%(\text{stat.}) \pm 0.16\%(\text{syst.}) \tag{4.2}$$

$$R_{\text{AD3}} = 84.67\% \pm 0.11\%(\text{stat.}) \pm 0.28\%(\text{syst.}) \tag{4.3}$$

$$R_{\text{AD4}} = 85.11\% \pm 0.31\%(\text{stat.}) \pm 0.29\%(\text{syst.}) \tag{4.4}$$

$$R_{\text{AD5}} = 85.11\% \pm 0.31\%(\text{stat.}) \pm 0.25\%(\text{syst.}) \tag{4.5}$$

$$R_{\text{AD6}} = 85.13\% \pm 0.31\%(\text{stat.}) \pm 0.28\%(\text{syst.}) \tag{4.6}$$

Figure 4.1 shows the H-Gd ratio with statistical error and systematical error for each AD. In this study, the H-Gd ratio and the average muon energy do not have significant correlations. Such a non-correlation agrees well with the result of Ref. [10].

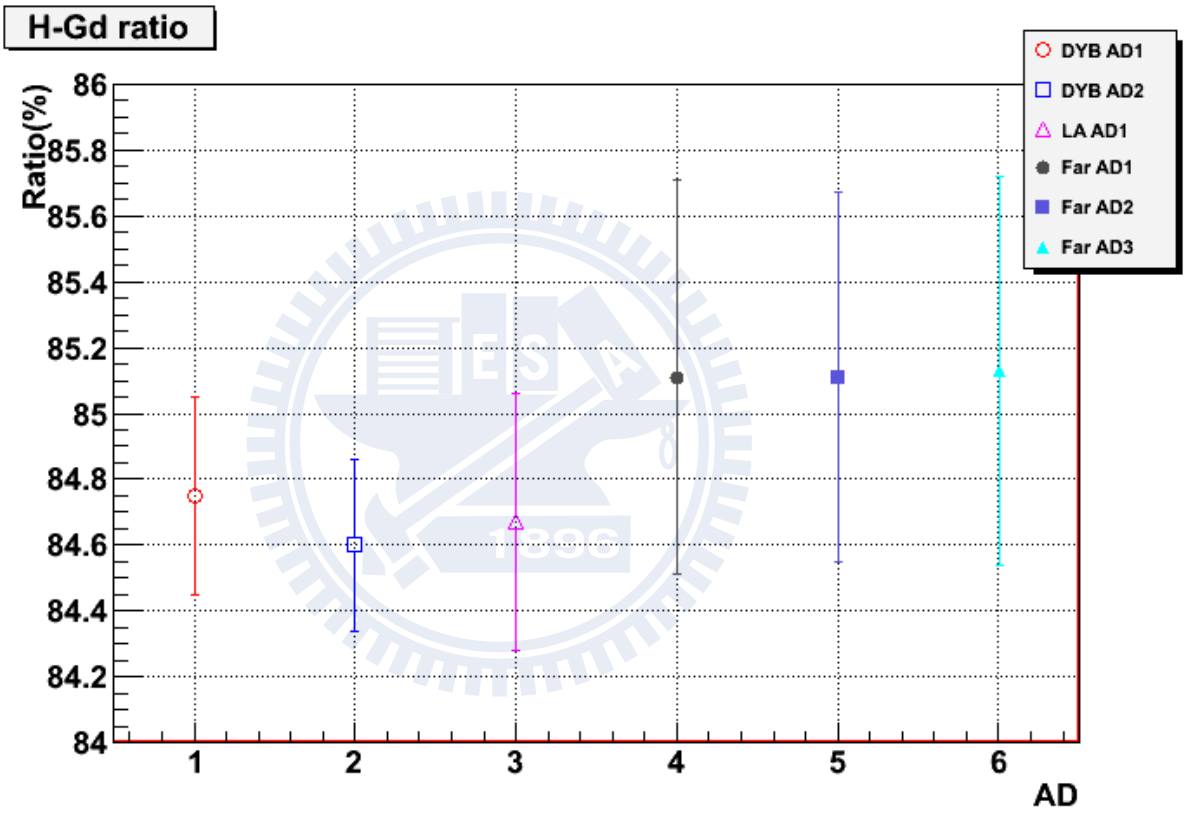

Figure 4.1: The H-Gd ratio with statistical error and systematical error for each AD.

Bibliography

[1] W. Pauli, Camb. Monogr. Part. Phys. Nucl. Phys. Cosmol. **14**, 1 (2000).

[2] J. Chadwick, Verh. Phys. Gesell. **16**, 383 (1914).

[3] D. Griffiths, Weinheim, Germany: Wiley-VCH (2008) 454 p.

[4] F. Reines, C. L. Cowan, F. B. Harrison, A. D. McGuire and H. W. Kruse, Phys. Rev. **117**, 159 (1960).

[5] G. Danby, J. M. Gaillard, K. A. Goulianos, L. M. Lederman, N. B. Mistry, M. Schwartz and J. Steinberger, Phys. Rev. Lett. **9**, 36 (1962).

[6] K. Kodama *et al.* [DONUT Collaboration], Phys. Lett. B **504**, 218 (2001).

[7] B. T. Cleveland, T. Daily, R. Davis, Jr., J. R. Distel, K. Lande, C. K. Lee, P. S. Wildenhain and J. Ullman, Astrophys. J. **496**, 505 (1998).

[8] F. P. An *et al.* [Daya Bay Collaboration], Nucl. Instrum. Meth. A **685**, 78 (2012).

[9] Daya Bay collaborators, Technical Design Review, second edition, 2008.

[10] Yung-Shun Yeh, *Measurement of the Neutron Yield Induced by Cosmic Muon in the Daya Bay Reactor Neutrino Experiment* , PhD thesis, National Chiao-Tung University, 2014.

[11] Y. F. Wang, V. Balic, G. Gratta, A. Fasso, S. Roesler and A. Ferrari, Phys. Rev. D **64**, 013012 (2001).

[12] X. Guo *et al.* [Daya-Bay Collaboration], hep-ex/0701029.

[13] F. P. An *et al.* [Daya Bay Collaboration], Chin. Phys. C **37**, 011001 (2013).

[14] B. Aharmim *et al.* [SNO Collaboration], Phys. Rev. C **81**, 055504 (2010).

[15] P. Adamson *et al.* [MINOS Collaboration], Phys. Rev. Lett. **106**, 181801 (2011).

[16] Gaosong Li, Jianglai Liu, *Absolute H-Gd Ratio Study with Spallation/AmC Neutrons* , Daya Bay Doc-7273, 2012.

[17] Bryce Littlejohn, *Center HGd Ratios from Spallation Neutrons: Redux for P12E* , Daya Bay Doc-9271, 2013.

[18] Feihong Zhang, *H-Gd ratio study with spallation neutron* , Daya Bay Doc-7554, 2012.

Appendix A

The Derivation of $\sigma'_{\mathbf{stat}}$

The ratio $R'_{\text{H-Gd}}$ with cut efficiency is defined as

$$R'_{\text{H-Gd}} = \frac{\frac{N_{\text{Gd}}}{\epsilon_{Gd}}}{\frac{N_{\text{Gd}}}{\epsilon_{\text{Gd}}} + \frac{N_{\text{H}}}{\epsilon_{\text{H}}}} = \frac{N'_{\text{Gd}}}{N'_{\text{Gd}} + N'_{\text{H}}}, \tag{A.1}$$

and

$$\frac{1}{R'_{\text{H-Gd}}} = 1 + \frac{N'_{\text{H}}}{N'_{\text{Gd}}} \tag{A.2}$$

$$\frac{N'_{\text{H}}}{N'_{\text{Gd}}} = \frac{1}{R'_{\text{H-Gd}}} - 1 = \frac{N_{\text{H}}}{N_{\text{Gd}}} \frac{\epsilon_{\text{Gd}}}{\epsilon_{\text{H}}} \tag{A.3}$$

$$\begin{aligned} \delta \frac{N'_{\text{H}}}{N'_{\text{Gd}}} &= \delta \frac{N_{\text{H}}}{N_{\text{Gd}}} \frac{\epsilon_{\text{Gd}}}{\epsilon_{\text{H}}} = \frac{\epsilon_{\text{Gd}}}{\epsilon_{\text{H}}} \delta \frac{N_{\text{H}}}{N_{\text{Gd}}} \\ &= \delta \frac{1}{R'_{\text{H-Gd}}} = \frac{-\delta R'_{\text{H-Gd}}}{{R'_{\text{H-Gd}}}^2} \end{aligned} \tag{A.4}$$

$$-\delta R'_{\text{H-Gd}} = \frac{\epsilon_{\text{Gd}}}{\epsilon_{\text{H}}} {R'_{\text{H-Gd}}}^2 \delta \frac{N_{\text{H}}}{N_{\text{Gd}}} \tag{A.5}$$

let

$$\frac{N_{\text{H}}}{N_{\text{Gd}}} = Z \tag{A.6}$$

$$\delta N_{\text{H}} = \sqrt{N_{\text{H}}} \tag{A.7}$$

$$\delta N_{\text{Gd}} = \sqrt{N_{\text{Gd}}} \tag{A.8}$$

thus

$$\begin{aligned} \frac{\delta Z}{Z} &= \sqrt{\left(\frac{\delta N_{\text{H}}}{N_{\text{H}}}\right)^2 + \left(\frac{\delta N_{\text{Gd}}}{N_{\text{Gd}}}\right)^2} \\ &= \sqrt{\frac{1}{N_{\text{H}}} + \frac{1}{N_{\text{Gd}}}} \end{aligned} \tag{A.9}$$

$$\begin{aligned} -\delta R'_{\text{H-Gd}} &= \frac{\epsilon_{\text{Gd}}}{\epsilon_{\text{H}}} {R'_{\text{H-Gd}}}^2 \frac{N_{\text{H}}}{N_{\text{Gd}}} \sqrt{\frac{1}{N_{\text{H}}} + \frac{1}{N_{\text{Gd}}}} \\ &= {R'_{\text{H-Gd}}}^2 \frac{N'_{\text{H}}}{N'_{\text{Gd}}} \sqrt{\frac{1}{N_{\text{H}}} + \frac{1}{N_{\text{Gd}}}} \\ &= {R'_{\text{H-Gd}}}^2 \left(\frac{1}{R'_{\text{H-Gd}}} - 1\right) \sqrt{\frac{1}{N_{\text{H}}} + \frac{1}{N_{\text{Gd}}}} \\ &= R'_{\text{H-Gd}} \left(1 - R'_{\text{H-Gd}}\right) \sqrt{\frac{1}{N_{\text{H}}} + \frac{1}{N_{\text{Gd}}}} \end{aligned} \tag{A.10}$$

$$\delta R'_{\text{H-Gd}} = R'_{\text{H-Gd}} \left(R'_{\text{H-Gd}} - 1\right) \sqrt{\frac{1}{N_{\text{H}}} + \frac{1}{N_{\text{Gd}}}} = \sigma'_{\text{stat}} \,. \tag{A.11}$$